UNC-CH-MATH-98/1

Folding the Square-Diagonal Lattice

P. Di Francesco*,

Department of Mathematics,
University of North Carolina at Chapel Hill,
CHAPEL HILL, N.C. 27599-3250, U.S.A.

We study the problem of "phantom" folding of the two-dimensional square lattice, in which the edges and diagonals of each face can be folded. The non-vanishing thermodynamic folding entropy per face $s \simeq .2299(1)$ is estimated both analytically and numerically, by successively mapping the model onto a dense loop model, a spin model and a new 28 Vertex, 4-color model. Higher dimensional generalizations are investigated, as well as other foldable lattices.

02/98 PACS: 64.60.-i Keywords: membrane, folding, entropy, vertex model

* e-mail: philippe@math.unc.edu

1. Introduction

Models for polymerized membranes can help our understanding of biological systems. A typical discretized model for a membrane consists of a network of vertices (atoms) linked by bonds. Irregular networks correspond to fluid membranes, with arbitrary connectivity at each vertex. Regular networks are called tethered membranes: their bonds may have short variations in length, leading to a geometrical crumpling transition [1]. Continuous versions of these models have confirmed this result, both analytically [2]-[4] and numerically [5]. In the present paper, we consider a discrete model for rigid bond-membranes, represented by regular 2-dimensional networks whose vertices are linked through rigid bonds of fixed length. The only possibility for such a membrane to modidy its spatial configuration is through folding along its bonds, serving as hedges between adjacent faces. The effects of self-avoidance on discrete folding models can be extremely complex: already in one dimension, this has lead to interesting developments, in relation with the "meander" problem [6]. The type of folding we consider however is not self-avoiding, in the sense that we allow the membrane to interpenetrate itself (phantom folding).

This work follows a previous study of the folding of the triangular lattice [7], leading to an exact result for the folding entropy in two dimensions [8], and to evidence for a first order folding transition between a flat and a folded phase [9], and some further developments in which the triangular lattice is folded into the 3-dimensional Face Centered Cubic lattice [10].

In this paper, we consider the folding problem of the square-diagonal lattice (see Fig.1 below), made of the square lattice with bonds joining all first and half of second-neighbor vertices. In a first step, we study the two-dimensional folding of the lattice and obtain estimates for its folding entropy. In a second step, we introduce d-dimensional generalizations in which the lattice is folded onto a regular d-dimensional lattice, allowing only for a finite number of possible relative foldings of adjacent faces of the membrane in the target d-dimensional space. Estimates for the higher-dimensional folding entropies are also found.

The paper is organized as follows. In Sect.2, we introduce the 2-dimensional folding problem of the square-diagonal lattice as an edge tangent-vector model. A reformulation as a colored loop model leads to some analytic bounds on the folding entropy. The structure of the colored loop model is further investigated in Sect.3, in relation with the Temperley-Lieb algebra and the Potts and 6 Vertex models. This leads to better analytic bounds

on the entropy. In Sect.4, we transform the colored loop model into a 28 Vertex model, allowing for the numerical study of the folding entropy, carried out in Sect.5.

The next two sections are devoted to higher dimensional generalizations of the square-diagonal lattice folding. The idea is to fold the lattice into a target d-dimensional lattice. We find two such lattices compatible with the square-diagonal lattice: the Hypercubic-Diagonal (HCD) and Face-Centered Hypercubic (FCH) lattices. The HCD model is studied in Sect.6, and successively mapped onto a colored loop model and a vertex model. Various estimates of the folding entropy follow. In Sect.7, an analogous study is carried out for the FCH model. The equivalent vertex model is particularly simple and gives access to very good numerical estimates of the folding entropy.

In Sect.8, we present a classification of all possible compactly foldable lattices in two dimensions. In addition to the known square and triangular lattices, we find only two more: the square-diagonal lattice studied in this paper, and the double-triangular lattice, a decoration of the triangular lattice obtained by adding vertices in the middle of one third of its edges (one per triangle), and by drawing the corresponding heights. The latter lattice is then folded in both 2 and higher dimensions, giving rise to new vertex models on the Kagomé lattice.

We gather a few concluding remarks in Sect.9.

2. The Folding Problem

2.1. Folding of the Square-Diagonal lattice

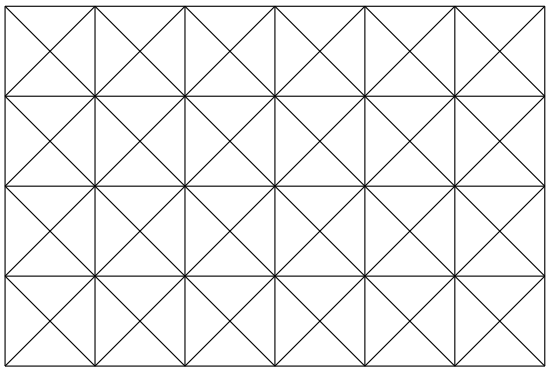

Fig. 1: The Square-Diagonal lattice. It has two types of vertices, respectively 4- and 8-valent, and two types of edges, short (length 1) and long (length $\sqrt{2}$).

We consider the *Square-Diagonal lattice*, obtained from the standard square lattice by drawing the two diagonals on each face (see Fig.1). This introduces two types of vertices, with respectively 4 and 8 incident edges, and two types of edges, short with length 1 and long with length $\sqrt{2}$. All the faces of the lattice are triangular, with one 4-vertex and two 8-vertices, and one long and two short edges forming a right angle.

The similarity of all the faces makes it possible to define a *complete folding* of the lattice, in which the edges serve as hinges between adjacent triangles, and might be either completely folded or not folded at all. A *folding configuration* of the lattice is therefore a continuous map ρ from the lattice to itself, which preserves its faces, namely the distances between the vertices around each triangular face. Note that a folding configuration does not distinguish between the various physical realizations of the actual folding of the lattice, nor is such a configuration granted to be realizable physically. This is called *phantom* folding, where the lattice is allowed to interpenetrate itself for the foldings to be realized, as opposed to the more realistic, but much more constrained *self-avoiding* folding.

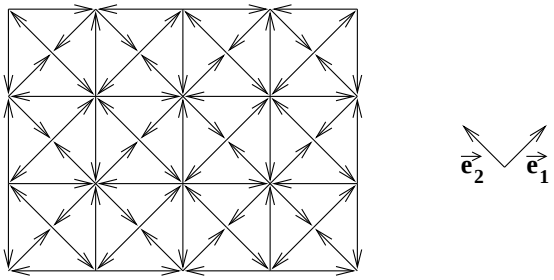

Fig. 2: The edge vectors for the square-diagonal lattice. In the basis $(\vec{e_1}, \vec{e_2})$, the short edge vectors are of the form $(\pm 1, 0), (0, \pm 1)$, and the long edge vectors are of the form $(\pm 1, \pm 1)$.

To describe the folding configurations of our lattice, we note that such a configuration is entirely determined by the list of all the images of the edges of the initial lattice. Let us characterize these edges by the associated tangent vectors $\vec{t}$, subject to the face rule

$$\sum_{\substack{\vec{t} \text{ around} \\ \text{a face}}} \vec{t} \;=\; \vec{0} \tag{2.1}$$

There are basically two choices of orientation of all the edge vectors, we fix one as in Fig.2. Fixing an orthogonal basis of the plane with two short vectors, denoted $\vec{e_1}$, $\vec{e_2}$, we see that the short edge vectors may only take the 4 values $\pm\vec{e_1}$ and $\pm\vec{e_2}$, whereas the long edge vectors may only take either of the 4 values $\pm\vec{e_1} \pm \vec{e_2}$.

A folding configuration is characterized by the images of these tangent edge vectors (note that short vectors are mapped to short vectors, and long vectors to long vectors). The requirement that the faces be preserved amounts to the condition that the face rule (2.1) be preserved by the map ρ. In other words,

$$\sum_{\substack{\vec{t} \text{ around} \\ \text{a face}}} \rho(\vec{t}) \;=\; \vec{0} \tag{2.2}$$

This condition has to be satisfied by the images of the edge vectors around all the faces of the lattice.

With these conditions, the partition function Z_{SD} of the folding problem of the square-diagonal lattice (actually of a portion thereof, made of N triangular faces) is simply the number of distinct folding configurations, namely of distinct configurations of edge vectors satisfying the conditions (2.2). The thermodynamic entropy per triangle s_{SD} is then defined as the limit

$$s_{SD} \;=\; \lim_{N\to\infty} \; \frac{1}{N} \mathrm{Log}\, Z_{SD} \tag{2.3}$$

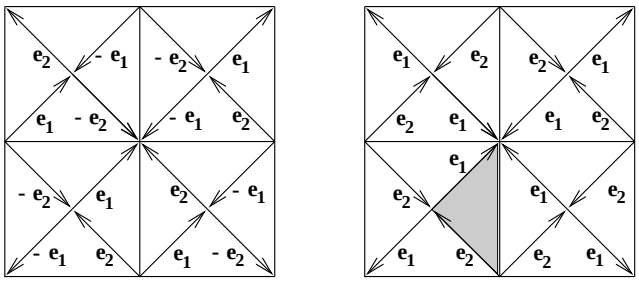

(a) **(b)**

Fig. 3: The short edge-vector images for the flat (a) and completely folded (b) configurations of the square-diagonal lattice. In case (b), the whole lattice is folded onto the shaded triangle.

With these definitions, we may already distinguish two particular folding configurations: the flat configuration corresponds to no folded edge, hence has the edge vectors of Fig.3(a). The completely folded configuration corresponds to folding the whole lattice onto one single of its triangular faces. The map therefore sends all the long edges onto one of them, say $-(\vec{e_1} + \vec{e_2})$ for definiteness, and half of the short edges to $\vec{e_1}$, the other half to $\vec{e_2}$, as shown on Fig.3(b).

2.2. Loop Gas Reformulation

Let us consider a folding configuration of the square-diagonal lattice. The images of the short edge vectors characterize the configuration completely, as the long edge vectors may be deduced from the face rules (2.1). But these are still constrained as follows.

(i) the two short edge vectors around each face must be perpendicular, i.e., one of them is equal to $\pm\vec{e_1}$ and the other to $\pm\vec{e_2}$.

(ii) any two adjacent triangular faces sharing a long edge have short edges with either of the two possible images below

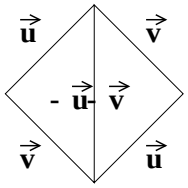

(2.4)

corresponding respectively to an unfolded or folded long edge.

The two conditions (i)-(ii) above are the only constraints on the images of the short edge vectors. The image of a given short edge vector $\vec{t}$ reads

$$\rho(\vec{t}) \;=\; \epsilon\vec{e_i} \tag{2.5}$$

and is characterized by the pair (i,ϵ), where $i \in \{1,2\}$ can be thought of as a *color* of the edge, and $\epsilon = \pm 1$ is a sign. In the condition (ii), the signs are the same for the short edges of the same color. Hence these signs are preserved along chains of short edges throughout the lattice, forming loops of either color 1 or 2.

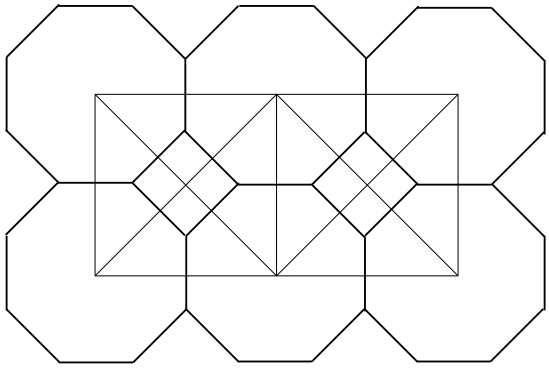

Fig. 4: The dual of the square-diagonal lattice (thick lines). The original square-diagonal lattice is represented in thin lines.

More precisely, let us consider the *dual* of the square-diagonal lattice, whose vertices are the centers of the triangular faces, and whose edges cross the former ones. This dual has only square and octagonal faces as depicted in Fig.4. The short edges are in bijective correspondence with the edges of the square faces in the dual lattice, hence we paint them with the corresponding colors $i = 1, 2$, which we will call black (solid lines in the pictorial representations) and white (dashed lines in the pictorial representations).

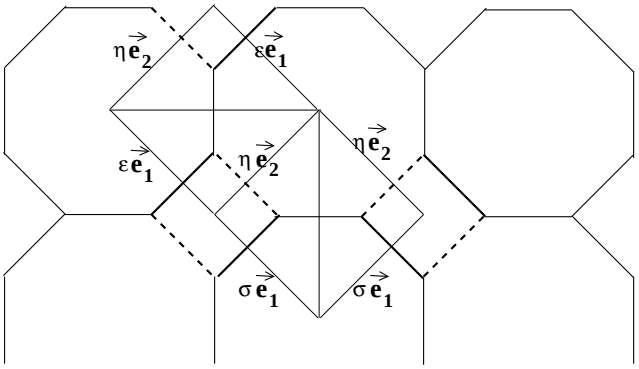

Fig. 5: A possible coloring of the dual of the short edges in black (thick solid lines) and white (thick dashed lines). The additional signs ϵ, η, σ of the corresponding short edge vectors are conserved on both sides of each long edge (thin long lines).

Around each square face of the dual, these colors must alternate, because of the condition (i). The two possibilities of (ii) simply correspond to the two *relative* colorings of the two corresponding neighboring dual square faces shown in Fig.5.

This suggests the following reformulation of the folding model, in the dual picture. We first choose an arbitrary configuration of the colorings of the edges around the square faces. There are two choices per square face. Such a configuration determines all the colors of all the short edges of the original lattice. We must now take care of the possible signs in (2.5). As we noted already, these signs propagate from short edge to short edge of the *same color*, between adjacent triangles sharing a long edge. It means that the sign remains the same along colored loops, formed by the edges of same color, connected in the dual lattice through a dual of long edge (namely an edge of octagon which is not an edge of square).

Let us now blow up the square faces of the dual and simultaneously shrink the duals of long edges, until the latter disappear, as shown in Fig.6. The octagonal faces become square faces, forming a checkerboard with the square faces with colored edges. We finally

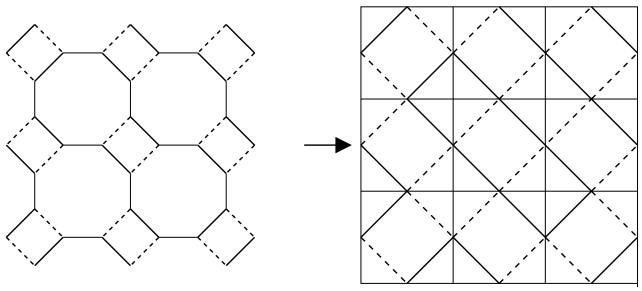

Fig. 6: We start from an arbitrary bicoloring of the dual of the short edges, in the dual lattice (a). We next blow up the square faces of the dual lattice and shrink the remaining octagon edges to zero, so as to get a (bicolored) square lattice (b). We have represented on (b) a new square lattice S in thin solid lines; each of its faces contains one bicolored square.

draw the square lattice (denoted by S) with vertices at the center of these new square faces (see Fig.6). The faces of this square lattice simply read either

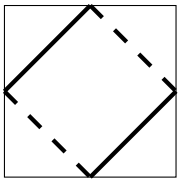

or

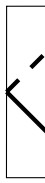

(2.6)

according to the previous coloring. Note that the black (resp. white) edges are connected between adjacent faces, thus forming lines across the lattice. Discarding the problem of boundary conditions, we may assume that the lattice geometry is toroidal (namely we consider a rectangle of size $P \times M$ of lattice, for a total of $N = 4PM$ triangular faces, with doubly periodic boundary conditions) and thus these lines form loops. The sign of (2.5) takes the same value along each such black or white loop. Denoting by N_b (resp. N_w) the numbers of black (resp. white) loops formed by the coloring configuration, the partition function of the folding problem of the square-diagonal lattice reads

$Z_{SD} =$ $\sum_{\text{coverings}}$

with 

(2.7)

where the coverings of the faces of S correspond to the various coloring configurations, and the factor 2 per black or white loop simply counts the possible choices of signs in (2.5).

We have therefore reformulated the folding problem as a dense loop gas problem, with a fugacity 2 per loop, and the presence of both loops (black) and their orthogonal trajectories (white).

2.3. Bounds and Expansions of the Folding Entropy

As an immediate consequence of (2.7), let us show that the square-diagonal lattice folding problem has a non-vanishing thermodynamic entropy s_{SD} (2.3). Indeed, we have the minoration

$$Z_{SD} \ \geq \ 2^{N/4} \tag{2.8}$$

obtained by counting the coloring configurations of the faces of S, i.e. a factor 2 per square. The factor $N/4$ follows from the fact that each square corresponds to 4 triangles in the original lattice. We therefore find

$$s_{SD} \ \geq \ \frac{1}{4}\mathrm{Log}\, 2 \ = \ .1732... \tag{2.9}$$

and the thermodynamic entropy does not vanish.

Another way would have consisted in choosing a particular coloring configuration of the faces of S, maximizing the number of black and white loops. This is readily obtained by letting the face configurations alternate between the two possibilities of (2.6) thus forming a checkerboard. Note that there are two such "groundstates", obtained from one another by exchanging the two face configurations. Restricting to one of these two colorings of S, we get the following minoration

$$Z_{SD} \geq 2^{N_b+N_w} \ = \ 2^{N/4} \tag{2.10}$$

where we have counted one (black or white) loop surrounding each vertex of S, hence a total number $N/4$. This again leads to (2.9).

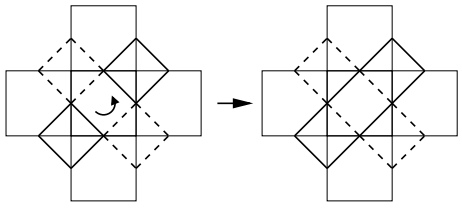

Fig. 7: A local excitation of a groundstate for Z_{SD}. It is obtained by flipping a face of S, while the rest of the groundstate configuration remains fixed. This creates 2 larger loops of black and white colors, by suppressing two minimal loops, one white and one black.

The advantage of this latter approach is to allow for a perturbative expansion of Z_{SD}, starting from one of the above groundstates, in terms of elementary local excitations. Such an excitation is simply the reversal of the coloring configuration of one face of S, as displayed in Fig.7. Doing this will affect the 4 loops (2 white, 2 black) surrounding the face, resulting in two larger loops, one black and one white. Overall this suppresses two loops, hence contributes an extra factor $1/4$ to the partition function. There are $N/4$ of these excitations, hence

$$Z_{SD} \;=\; 2^{N/4}(1+\frac{1}{4}\frac{N}{4}+...) \tag{2.11}$$

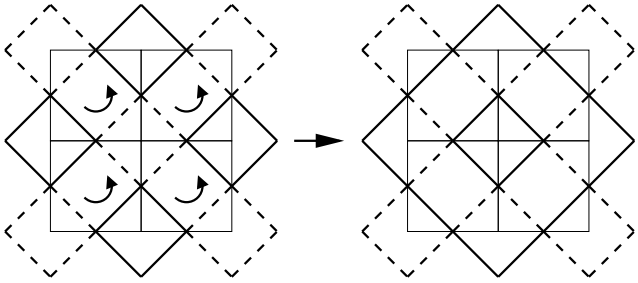

Fig. 8: The four elementary excitations forming a 2×2 square. These replace 4 black and 5 white loops by 1 white and 2 black ones, resulting in a relative weight $1/2^6$ instead of the expected $1/2^8$ for four distant local excitations. The role of black and white loops is exchanged when the four excitations are shifted by one face.

This expansion can be continued for higher numbers of excitations, but these might interact, by creating or suppressing more loops when they are close together than when they are separated. The first instance of this occurs for 4 excitations. Generically, 4 excitations will contribute an extra factor of $1/2^8$ to the partition function, except when these form a 2×2 square, as illustrated in Fig.8. Indeed, in that case, a loop is created in the center of this square, and the factor is increased to $4/2^8 = 1/2^6$. This is interpreted as a contact interaction energy between the excitations. This phenomenon propagates to higher orders. For instance, this is further increased when 6 excitations form a 2×3 or 3×2 rectangle, resulting in a factor $1/2^8$ instead of the expected $1/2^{12}$ if excitations did not interact. Up to 6 excitations, the contributions to Z_{SD} read (for convenience, we set

$N/4 = n$)

$$
\begin{aligned}
Z_{SD} \;=\; & 2^n \Big(1 + \frac{n}{2^2} + \binom{n}{2}\frac{1}{2^4} + \binom{n}{3}\frac{1}{2^6} + \big[\binom{n}{4}\frac{1}{2^8} + n(\frac{1}{2^6} - \frac{1}{2^8})\big] \\
& + \big[\binom{n}{5}\frac{1}{2^{10}} + n(n-4)(\frac{1}{2^8} - \frac{1}{2^{10}})\big] \\
& + \big[\binom{n}{6}\frac{1}{2^{12}} + n\frac{(n-4)(n-5)}{2}(\frac{1}{2^{10}} - \frac{1}{2^{12}}) + 2n(\frac{1}{2^8} - \frac{2}{2^{10}})\big] + ... \Big)
\end{aligned}
\tag{2.12}
$$

The first line of (2.12) includes terms up to four excitations. The bracket includes the replacement of the expected $1/2^8$ term by the actual $1/2^6$ explained above. This occurs with a degeneracy n, corresponding to the freedom of moving the center of the 2×2 excitation on the lattice. The second line in (2.12) corresponds to 5 excitations. Again, we have replaced the expected $1/2^{10}$ by $1/2^8$ whenever a 2×2 excitation is formed, together with another single excitation. Those arise with a multiplicity $n(n-4)$. Finally, the third line of (2.12) corresponds to 6 excitations. We have first replaced the expected $1/2^{12}$ by $1/2^{10}$ whenever a 2×2 excitation is formed, together with two other single excitations. This occurs with the multiplicity $n \times (n-4)((n-5)/2$, for the choice of the center of the 2×2 excitation among n vertices, and the pair of remaining excitations among the remaining $(n-4)$ faces. But doing so we have neglected the occurrence of 2×3 and 3×2 rectangular excitations, for which the previous $1/2^{10}$ must be replaced by $1/2^8$. This occurs $2n$ times (n per rectangular shape), but we have to subtract all the terms in which these rectangles have been counted as a 2×2 square plus two excitations, namely $4n$ terms with weight $1/2^{10}$. We deduce the following Mayer expansion of the thermodynamic entropy

$$
s_{SD} \;=\; \frac{1}{4}\mathrm{Log}(2(1 + \frac{1}{4} + \frac{3}{4^4} - \frac{9}{4^5} + \frac{18}{4^6} + \frac{1}{4^4} + ...)) = \simeq \; .231... \tag{2.13}
$$

(i.e. a partition function per triangle of $z_{SD} \simeq 1.259...$) including the effects of up to 6 local excitations. Note that there are negative and positive terms in the expansion (2.13), so it is not clear whether this estimate lies above or below the exact value of s_{SD}. It is possible however to prove that the first two terms give a strict lower bound on the entropy. This indeed amounts to neglecting the interactions between the excitations, hence to underestimate Z (as we under-count the loops). We therefore get a first lower bound

$$
s_{SD} \;>\; \frac{1}{4}\mathrm{Log}(\frac{5}{2}) \;=\; .22907... \tag{2.14}
$$

corresponding to a partition function per triangle of 1.2574...

3. Loops and the Temperley-Lieb Algebra

3.1. The Dense Loop Gas

The formulation of the square-diagonal folding problem as a coloring problem has left us with a gas of dense black and white loops, each weighed by a factor of 2.

Here, we recall some known facts about the dense loop gas on the square lattice S. The idea is to generate a dense set of black loops on S, in the same way as we did for black and white loops, except that all the dashed lines are erased. Each loop is weighed by a factor β, resulting in a partition function

$Z_\beta \; =$

(3.1)

where L denotes the number of loops formed by the black lines.

The model is intimately related to both Q states Potts and 6 Vertex models at infinite temperature, in that it has a straightforward definition in terms of the Temperley-Lieb algebra [11]. Indeed, let us introduce the abstract "face" operator

$e_i \; =$

$$= \; 1 \otimes 1 \otimes \cdots \otimes 1 \otimes e \otimes 1 \otimes \cdots \otimes 1 \tag{3.2}$$

acting on a row of $2P$ parallel black lines. In (3.2), the face operator e acts on the i-th and $(i+1)$-th lines, by connecting them. The definition (3.2) makes transparent the following algebraic relations satisfied by the e_i's

$$\begin{aligned} e_i^2 &= \beta \, e_i \\ e_i e_{i\pm 1} e_i &= e_i \\ e_i e_j &= e_j e_i \quad \text{for } |i-j| > 1 \end{aligned} \tag{3.3}$$

easily checked pictorially. The algebra generated by the abstract generators $1, e_1, e_2, ..., e_{2P-1}$, subject to (3.3), is called the Temperley-Lieb algebra, denoted by $TL_{2P}(\beta)$.

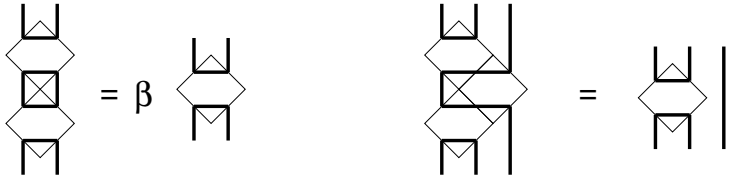

Fig. 9: The first and second relation of (3.3).

The first relation in (3.3) is consistent with the weight β per loop in (3.1): as shown in Fig.9, we can erase the loop formed by e_i^2 and replace it by a factor β. The second relation expresses than one can "pull" the black lines, as illustrated in Fig.9. The last relation simply expresses the locality of the action of the face operator at lines i and $i+1$.

To write the partition function of the dense loop model, we introduce a diagonal zigzag-to-zigzag transfer matrix

$$\begin{aligned} T_\beta &= U_\beta \, V_\beta \\ U_\beta &= \prod_{i=1}^{P-1} (1+e_{2i}) \\ V_\beta &= \prod_{i=1}^{P} (1+e_{2i-1}) \end{aligned} \tag{3.4}$$

The partition function of the model on a strip of width $2P$ and height $2M$, counted in numbers of lines (with $N = 4PM$, as the total number of faces of S is $N/4 = PM$), with periodic conditions along its width $2P$ boundaries reads

$$Z_\beta = \mathrm{Tr}(T^M) \tag{3.5}$$

where the trace is the standard trace on the Temperley-Lieb algebra, defined recursively by $\mathrm{Tr}(1) = \beta^{2P}$ and the recursion relation (Markov property)

$$\mathrm{Tr}\big(e_{i+1} E(e_1, e_2, ..., e_i)\big) \;=\; \frac{1}{\beta} \mathrm{Tr}\big(E(e_1, e_2, ..., e_i)\big) \tag{3.6}$$

for any expression E depending on the e_k, $k \leq i$ only. With this definition, (3.5) is calculated by simply first expanding T^M as a sum of products of e's, then by identifying the black lines along the width $2P$ boundaries, and replacing each black loop by a factor of β, thus realizing exactly the sum in (3.1). The dense loop gas partition function (3.5) coincides with that of the square lattice isotropic Q-states Potts model at its critical temperature, with $\beta = \sqrt{Q}$ [12].

The abstract definition (3.3) of the algebra of the e's makes it possible to calculate (3.5) by choosing a particular representation for the algebra. A particular choice relates it to the partition function of the 6 Vertex model [12], solved with standard Bethe Ansatz techniques. This gives an exact formula for the thermodynamic entropy per site of the dense loop model [12]

$$s_\beta \;=\; \begin{cases} \int_{-\infty}^{\infty} \frac{\sinh(\pi-\mu)x \;\tanh \mu x}{2x \;\sinh \pi x} & \text{for} \quad \beta = 2\cos\mu, \quad 0 < \mu < \pi \\ \frac{\lambda}{2} + \sum_{n=1}^{\infty} \frac{e^{-n\lambda}}{n} \tanh n\lambda & \text{for} \quad \beta = 2\cosh\lambda, \quad \lambda > 0 \\ 2 \;\mathrm{Log}\, \frac{\Gamma(\frac{1}{4})}{2\Gamma(\frac{3}{4})} & \text{for} \quad \beta = 2 \end{cases} \tag{3.7}$$

This takes care of all the values of $\beta \geq 0$. Note that there are $N/4$ sites in the model, as there are 4 triangles of the original square-diagonal lattice on each face of S. The entropies *per triangle* are therefore those of (3.7) divided by 4.

3.2. More Bounds on the Folding Entropy

As the dense loop model (3.1) is obtained by dropping the white loop contributions to the square-diagonal folding model (2.7), we get a minoration of the thermodynamic entropy (2.3)

$$s_{SD} \;>\; \frac{1}{4}\, s_{\beta=2} \;=\; \frac{1}{2}\,\mathrm{Log}\,\frac{\Gamma(\frac{1}{4})}{2\Gamma(\frac{3}{4})} \;=\; .19579... \tag{3.8}$$

as there are 4 triangles of the original lattice per vertex of S. This is below our first estimate (2.13), and our previous lower bound (2.14).

We can also find an upper bound for the folding entropy s_{SD}, by noticing that the maximum possible number of white loops is obtained in one of the two abovementioned groundstates, hence $N_w \leq N/8$ in all configurations. Using (2.7), we arrive at

$Z_{SD} \;<\; 2^{N/8}$

with

co

(3.9)

hence the upper bound on the folding entropy

$$s_{SD} \;<\; \frac{1}{8}\log 2 + \frac{1}{4} s_2 \;=\; .28244... \tag{3.10}$$

This lies above our first estimate (2.13).

This bound can be improved greatly by using the Hölder inequality for averages, namely

$$\langle AB \rangle \;\leq\; \langle A^\mu \rangle^{\frac{1}{\mu}} \langle B^\nu \rangle^{\frac{1}{\nu}} \tag{3.11}$$

where μ, ν are two positive real numbers subject to $1/\mu + 1/\nu = 1$, and A, B are two observables averaged over a set of configurations $\mathcal{C}$: $\langle A \rangle = (\sum_{c \in \mathcal{C}} A(c))/|\mathcal{C}|$. We may apply (3.11) to the sum over bi-coloring configurations of the faces of S, with the observables $A(c) = 2^{N_b}$ and $B(c) = 2^{N_w}$. It is easy to see that the lowest upper bound corresponds to $\mu = \nu = 2$, with the result

$Z_{SD} \;\leq$

$\sum$

coverings

c

with

(3.12)

where we have identified the partition function of the dense loop model (3.1) at $\beta = 4$. Using (3.7), we find that $2\cosh\lambda = 4$, hence $\lambda = \mathrm{Log}(2+\sqrt{3})$, and we have the upper bound on the folding entropy

$$\begin{aligned} s_{SD} \;&\leq\; \frac{1}{4}s_4 \;=\; \frac{1}{8}\mathrm{Log}(2+\sqrt{3}) \\ &+ \frac{1}{4}\sum_{n=1}^{\infty}\frac{1}{n(2+\sqrt{3})^n}\frac{(2+\sqrt{3})^{2n}-1}{(2+\sqrt{3})^{2n}+1} \;=\; .23352... \end{aligned} \tag{3.13}$$

corresponding to a partition function per triangle of 1.2630...

Note that this upper bound only exceeds our Mayer expansion estimate by 1/2%. The dense loop model at $\beta = 4$ is therefore a good approximation of the square-diagonal folding problem, as far as the entropy is concerned. This is best seen by examining the relative numbers of black and white loops in the sum (2.7). In the groundstates, $N_b = N_w = N/8$. The first excitations (up to 3) preserve $N_b = N_w$, but change their value. The first relative change of N_b and N_w is obtained for 4 excitations, when they form a 2×2 square (c.f. the Mayer expansion (2.13)). According to whether the central loop is black or white, we get $N_b = N_w \pm 2$. However, we expect in average the numbers of black and white loops to be sensibly the same. This explains why $Z_{\beta=4}$ is a good approximation of Z_{SD}, which amounts to simply replacing the summand $2^{N_b+N_w}$ in (2.7) by $2^{2N_w} = 4^{N_w}$.

3.3. Black and White Loops

The full black and white loop model (2.7) can be expressed in terms of *two* coupled Temperley-Lieb algebras, one for each color of loop. Let us slightly generalize (2.7) into

$$Z_{\beta,\bar\beta} \;=\; \sum_{\text{coverings}\ c} \beta^{\#\text{ black loops of }c}\,\bar\beta^{\#\text{ white loops of }c} \tag{3.14}$$

with

by affecting a weight β per black loop and $\bar\beta$ per white loop.

Tilting the lattice S by 45 degrees, we are led to the introduction of the following face

operators:

e_i =

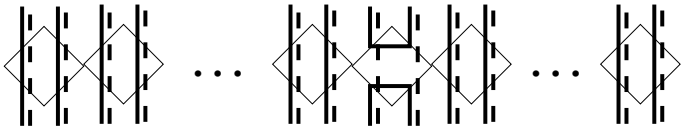

$$= (1 \otimes 1) \otimes ... \otimes (1 \otimes 1) \otimes (e \otimes 1) \otimes (1 \otimes 1)...(1 \otimes 1)$$

f_i =

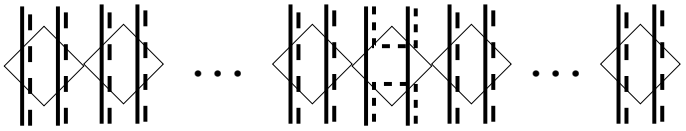

$$= (1 \otimes 1) \otimes ... \otimes (1 \otimes 1) \otimes (1 \otimes e) \otimes (1 \otimes 1)...(1 \otimes 1) \tag{3.15}$$

acting on a set of $2P$ pairs of black and white parallel lines (in each parenthesis of (3.15), the first term of the tensor product corresponds to the black lines and the second one to the white lines). It is clear from the discussion of the previous section that the e_i satisfy the relations (3.3) of the Temperley-Lieb algebra $TL_{2P}(\beta)$, whereas the f_i satisfy those of $TL_{2P}(\bar{\beta})$. In addition, we have the commutation relations $[e_i, f_j] = 0$ for all i and j.

Let us introduce the zigzag-to-zigzag transfer matrix

$$\begin{aligned} T &= U\ V \\ U &= \prod_{i=1}^{P} (e_{2i} + f_{2i}) \\ V &= \prod_{i=1}^{P} (e_{2i-1} + f_{2i-1}) \end{aligned} \tag{3.16}$$

acting on a row of $2P$ pairs of parallel black and white lines, and reproducing the two possible face colorings (2.6). The partition function for a portion of size $2P \times 2M$ of the square-diagonal lattice can be finally expressed as

$$Z_{\beta,\bar{\beta}} = \mathrm{Tr}(T^M) \tag{3.17}$$

by imposing periodic conditions along the width $2P$ zigzag boundaries, namely by identifying all black and white lines along those. In (3.17), the trace is defined for a tensor product of any two elements $E \in TL_{2P}(\beta)$ and $F \in TL_{2P}(\bar{\beta})$ as $\mathrm{Tr}(E \otimes F) = \mathrm{Tr}(E)\ \mathrm{Tr}(F)$, and extended by linearity.

The remark of the previous section about the independence of Z_β on the particular representation chosen for e_i is still valid here, and extends to the choice of representation

for f_i as well. This would enable us for instance to map the model onto a pair of coupled 6 Vertex models. We will find an equivalent 28 Vertex model in the next section.

Comparing the expression (3.16) for the transfer matrix to that of the dense loop model (3.4), we note that

$$\begin{aligned} e_i + f_i &= \frac{1}{2}\big((1+e_i)(1+f_i) - (1-e_i)(1-f_i)\big) \\ &= \frac{1}{2}\sum_{\sigma_i=\pm 1} \sigma_i(1+\sigma_i e_i)(1+\sigma_i f_i) \end{aligned} \tag{3.18}$$

This suggests to define a multi-parameter transfer matrix for the dense loop model, namely

$$\begin{aligned} T_\beta(x_1, x_2, ..., x_{2P-1}) &= U_\beta(x_2, , x_4..., x_{2(P-1)}) V_\beta(x_1, x_3, ..., x_{2P-1}) \\ U_\beta(x_2, x_4..., x_{2(P-1)}) &= \prod_{i=1}^{P-1}(1 + x_{2i}e_{2i}) \\ V_\beta(x_1, x_3, ..., x_{2P-1}) &= \prod_{i=1}^{P}(1 + x_{2i-1}e_{2i-1}) \end{aligned} \tag{3.19}$$

so that

$$T = \sum_{\substack{\sigma_i=\pm 1 \\ i=1,2,\ldots,2P-1}} \left(\prod_{i=1}^{2P-1} \frac{\sigma_i}{2}\right) T_\beta(\sigma_1, \sigma_2, ..., \sigma_{2P-1}) T_{\bar\beta}(\sigma_1, \sigma_2, ..., \sigma_{2P-1}) \tag{3.20}$$

The matrices $T_\beta(x) = T_\beta(x, x, ..., x)$ commute with each other for distinct values of x, as a consequence of the Yang-Baxter equation [12]. Unfortunately, we have not been able to use this fact to "baxterize" the matrix T by introducing a spectral parameter x, so as to form a family of commuting transfer matrices $T(x)$. This is because the matrices $T_\beta(\sigma_1 x, ..., \sigma_{2P-1}x)$ do not commute with each other for arbitrary values of the σ_i's. So the expression (3.20) cannot be used to diagonalize T in an efficient manner.

4. An Equivalent 28 Vertex Model

4.1. Spin Model

The square-diagonal folding problem in its final form can be rewritten as a *spin* model as follows. To each edge of the square lattice S, we attach two spin variables $\sigma, \tau \in \{-1, 1\}$. These stand for the two signs attached to the black and white lines passing through the center of the edge. These spins interact around each face of S, because of spin conservations

imposed by either of the two face colorings (2.6). More precisely, each configuration of spins (σ, τ) around a face of S receives the Boltzmann weight

w 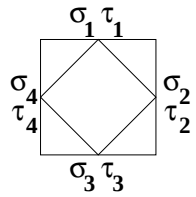

$= \delta_{\sigma_1}$

$+ \delta_{\sigma_1,}$

(4.1)

where the two contributions correspond to the two possible colorings of the face.

This formulation permits to define a row-to-row transfer matrix for the model on a strip of width P, namely

$$T_{\{(\sigma_i,\tau_i)\},\{(\sigma'_i,\tau'_i)\}} = \sum_{\substack{s_i,t_i=\pm 1 \\ i=1,2,..,P+1}} \prod_{i=1}^{P} w \Bigg(\quad$$ 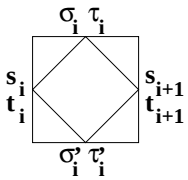

(4.2)

4.2. 28 Vertex Model

We will now rewrite the Boltzmann weight (4.1) in terms of a "color" variable $a \in \mathbb{Z}_4$, defined on the edges of the dual S^* of the square lattice S. Namely, we replace each spin configuration around the faces of S by a coloring configuration of the edges adjacent to the corresponding dual vertex

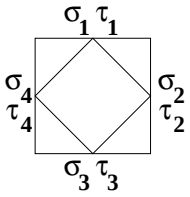

$\rightarrow$ **a**

(4.3)

with the correspondence

$$\begin{aligned} (\sigma, \tau) &\rightarrow a \\ (+,+) &\rightarrow 0 \\ (+,-) &\rightarrow 1 \\ (-,-) &\rightarrow 2 \\ (-,+) &\rightarrow 3 \end{aligned} \tag{4.4}$$

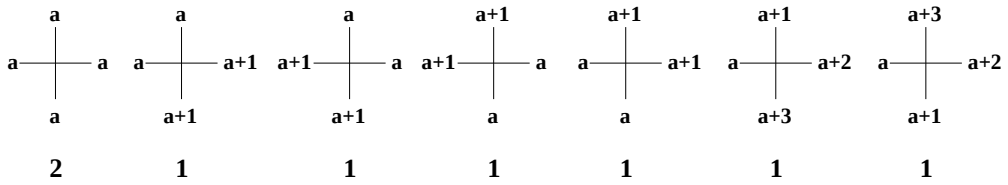

Fig. 10: The 28 possible vertices corresponding to the spin configurations of (4.1). The color a may take any value $0, 1, 2, 3$ modulo 4. The corresponding Boltzmann weight is indicated below each vertex.

By inspection of all the possibilities in (4.1), we are left with the only possible vertices of Fig.10, with $a = 0, 1, 2, 3$. This gives a total of $4 \times 7 = 28$ distinct vertices. Note that the first vertex of Fig.10 corresponds to $\sigma_1 = \sigma_2 = \sigma_3 = \sigma_4$ and $\tau_1 = \tau_2 = \tau_3 = \tau_4$ for all a, hence the corresponding Boltzmann weight receives contributions from both terms of (4.1). This accounts for the Boltzmann weight 2. All other coloring configurations have weight 1, as only one of the two terms in (4.1) is selected.

The row-to-row transfer matrix (4.2) can be reexpressed as a row-to-row transfer matrix for the 28 Vertex model

$$T_{\{a_i\},\{a'_i\}} \;=\; \sum_{\substack{b_i \in \mathbb{Z}_4 \\ i=1,2,..,P+1}} \prod_{i=1}^{P} w \left(\quad \begin{array}{ccc} & \mathbf{a_i} & \\ \mathbf{b_i} & & \mathbf{b_{i+1}} \\ & \mathbf{a'_i} & \end{array} \right) \tag{4.5}$$

In view of trying to solve our original folding problem, we tried to find an integrable structure underlying the 28 Vertex model of Fig.10, allowing for distinct Boltzmann weights $w_1, w_2, .., w_7$ for each of the 7 ($\times 4$) vertices. It appears that no non-trivial solutions to the Yang-Baxter equation can be found here. Moreover, our special case $w_1 = 2$, $w_2 = ... = w_7 = 1$ appears to be very singular. Indeed, the 12×12 R-matrix with entries

$$R_{(a,b);(a',b')} \;=\; w \left(\quad \begin{array}{ccc} & \mathbf{b} & \\ \mathbf{a} & & \mathbf{b'} \\ & \mathbf{a'} & \end{array} \right) \tag{4.6}$$

is not invertible at that point (note that $b = a, a \pm 1$ in (4.6), hence the size is 12 instead of 16).

Although the matrix (4.5) displays an interesting block structure, it does not seem to be diagonalizable in a nice and systematic way.

5. Numerical Studies

This leaves us with little but the possibility of a numerical study, which we will carry out in this section. This is particularly efficient because T is a sparse matrix. Indeed, there are approximately 7^N non-vanishing matrix elements in T (given the color of the western edge of a vertex, there are exactly 7 possibilities for the northern, eastern and southern edges), whereas T is a $4^N \times 4^N$ matrix, hence a ratio of non-vanishing elements of $(7/16)^N$.

The results of the following subsections have been obtained by

(i) constructing the transfer matrix T of the 28 Vertex model, including the appropriate boundary conditions

(ii) determining the block structure of T

(iii) extracting the largest eigenvalue of T in the dominant block, by iteration of the action of T on an initial vector v_0, normalized at each step: this process converges nicely to the Perron-Frobenius eigenvector of the matrix.

The particularity of the model gives us the possibility of generating the matrix elements of T "linearly", by simply listing all its non-vanishing entries (hence a list of length $\simeq 7^n$). Indeed, for each sequence of n vertices in the list (each of which is chosen among the 7 possibilities of Fig.10), the values of the bottom and top vertical edge images are completely fixed. Conversely, a given pair (bottom,top) of vertical edge configurations corresponds to at most one such arrangement of n vertices. This enables us to encode all of T in a vector of length $\simeq 7^n$, and to use it directly for determining the largest eigenvalue λ_{max}.

The various choices of boundary conditions are:

(1) periodic, by identifying the west-most and east-most edges of the row

(2) fixed, by setting to the value 0 both west-most and east-most edges of the row

(3) mixed, by fixing the east-most edge value to 0, and summing over all west-most edge values. This latter case is also equivalent to having free boundary conditions on both ends.

5.1. Periodic Boundary Conditions

n	size	$\lambda_{\max}$	$\lambda_{\max}^{1/(4n)}$
1	1	2.	1.18920
2	4	10.	1.33352
3	16	12.9282	1.23773
4	36	48.9317	1.27526
5	256	83.9919	1.24799
6	400	285.092	1.26558
7	4096	539.435	1.25189

Table I: Numerical results for the transfer matrix of the 28 Vertex model with periodic boundary conditions. We list the length n of the row, the size of the relevant block of the transfer matrix to be diagonalized, the largest eigenvalue $\lambda_{\max}$, and the sequence $\lambda_{\max}^{1/(4n)}$, converging to the partition function per triangle. Note the parity effect on this sequence, which gives a framing of the actual limit.

We display in Table I the results for the largest eigenvalue of the transfer matrix T for periodic boundary conditions. We note the usual oscillatory behavior of the approximation to the partition function per site, namely $\lambda_{\max}^{1/(4n)}$. This makes extrapolation more difficult, as we must distinguish between both parities of n, and we rather rely on the other types of boundary conditions for a better behavior.

5.2. Fixed Boundary Conditions

n	size	$\lambda_{\max}$	$\lambda_{\max}^{1/(4n)}$	ν_n
1	1	2.0000000	1.18920	
2	3	4.5615528	1.20889	1.22891
3	7	10.898979	1.22025	1.24327
4	22	26.562737	1.22748	1.24945
5	69	65.399363	1.23247	1.25263
6	236	161.98393	1.23612	1.25451
7	800	402.76893	1.23890	1.25572
8	2850	1004.1851	1.24109	1.25657

Table II: Numerical results for the transfer matrix of the 28 Vertex model with fixed boundary conditions (= 0 on both ends). We list the length n of the row, the size of the relevant block of the transfer matrix to be diagonalized, the largest eigenvalue $\lambda_{\max}$, and two sequences converging to the partition function per triangle, namely $\lambda_{\max}^{1/(4n)}$, and $\nu_n = (\lambda_{n+1}/\lambda_n)^{1/4}$.

We display in Table II the results for the largest eigenvalue of the transfer matrix T for fixed boundary conditions to the value 0 on both ends of the row. It turns out that the block which dominates T is that containing the row-configuration $[0, 0, 0, ..., 0]$ of n edges (it gives access to the largest entry of T, namely $T_{[0...0],[0...0]} = 2^n$). The size of this block is indicated in Table II. The sequence ν_n of consecutive ratios of eigenvalues is strictly increasing, and gives a good extrapolation using the Aitken algorithm (exponential fit). We find

$$z_{SD} \;=\; e^{s_{SD}} \;\simeq\; 1.258(1) \qquad \Rightarrow \qquad s_{SD} \;\simeq\; .230(1) \tag{5.1}$$

5.3. Mixed Boundary Conditions

n	size	$\lambda_{\max}$	$\lambda_{\max}^{1/(4n)}$	ν_n
1	3	3.0000000	1.316074	
2	12	7.7184785	1.291045	1.266492
3	48	19.490918	1.280213	1.260593
4	192	48.985790	1.275350	1.259097
5	768	122.95423	1.272000	1.258688
6	3072	308.55772	1.269762	1.258630
7	12288	774.49976	1.268175	1.258697
8	49152	1944.7242	1.267000	1.258807

Table III: Numerical results for the transfer matrix of the 28 Vertex model with mixed boundary conditions (= 0 on one end, free on the other). We list the length n of the row, the size of the relevant block of the transfer matrix to be diagonalized, the largest eigenvalue $\lambda_{\max}$, and two sequences converging to the partition function per site, namely $\lambda_{\max}^{1/(4n)}$, and $\nu_n = (\lambda_{n+1}/\lambda_n)^{1/4}$.

We display in Table III the results for the largest eigenvalue of the transfer matrix T for mixed boundary conditions, fixed at 0 on one end, and free on the other. Note that the size of the matrix to be diagonalized is the full size of T, $3 \times 4^{n-1}$. On the other hand, the

sequence ν_n of consecutive ratios of eigenvalues displays a very nice convergence. Using the abovementioned extrapolation scheme, we arrive at

$$z_{SD} \;=\; e^{s_{SD}} \;\simeq\; 1.2586(1) \qquad \Rightarrow \qquad s_{SD} \;\simeq\; .2299(1) \tag{5.2}$$

Note that this result is slightly smaller than the Mayer estimate (2.13).

6. d-Dimensional Hypercubic-Diagonal Folding

6.1. Discrete Folding in Higher Dimensions

In the present paper, we have studied the *two-dimensional* folding of the square-diagonal lattice, in which the image of the folding maps ρ is a subset of the original lattice. If we relax the latter constraint, we may just consider maps from the original lattice to say $\mathbb{R}^d$. It is however desirable that the target configurations may only have finitely many possibilities to form local folds, i.e. we should not allow folds with arbitrary angles. We may introduce a higher-dimensional *discrete* folding problem by simply demanding that the image of the folding maps ρ, subject to (2.2), be a subset of a d-dimensional lattice [10]. This is possible only if the d-dimensional "target" lattice is compatible with the square-diagonal lattice, in the sense that such d-dimensional folding configurations indeed exist.

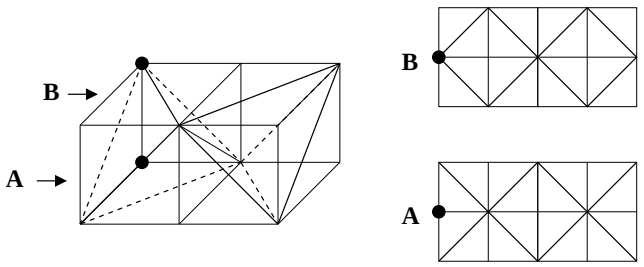

Fig. 11: The unit cell of the Hypercubic-Diagonal lattice of dimension $d = 3$. The horizontal plane sections alternate between the A and B types of square-diagonal lattice as we move along the vertical. This holds for any other plane sections perpendicular to a basis vector.

We have found two such compatible choices of lattice. The first choice consists of the d-dimensional Hypercubic-Diagonal (d-HCD) lattice (represented in Fig.11 for $d = 3$), generated by the orthonormal vectors $\vec{e_1}$, $\vec{e_2}$, ..., $\vec{e_d}$, $|\vec{e_i}| = 1$ (with "short" edges of length 1), together with exactly one of the diagonals on each of its 2-dimensional faces (the "long"

edges, of length $\sqrt{2}$). These diagonals are chosen so that none of them contains the origin of the lattice, and that each plane section of the lattice, parallel say to $(\vec{e_i}, \vec{e_j})$, $1 \leq i < j \leq d$, is a copy of the square-diagonal lattice, with an alternance of A and B-types (c.f. Fig.11) as we move along a direction $\vec{e_k}$, perpendicular to $(\vec{e_i}, \vec{e_j})$. Note that on the lattice, any two short edges are either parallel or perpendicular. The sub-lattice of the HCD formed by erasing all short edges was also considered for the d-dimensional folding of the triangular lattice in [10].

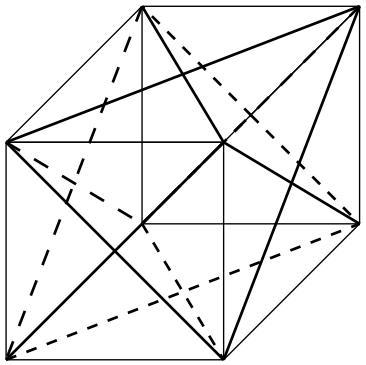

Fig. 12: The unit cell of the d-dimensional Face-Centered Hypercubic lattice for $d = 3$.

The other is the d-dimensional Face-Centered Hypercubic (FCH) lattice (represented in Fig.12 for $d = 3$), namely the d-dimensional hypercubic lattice generated by orthogonal vectors $\vec{f_1}$, $\vec{f_2}$, ..., $\vec{f_d}$, $|\vec{f_i}| = \sqrt{2}$ (with "long" edges of length $\sqrt{2}$), together with the two diagonals on each of its 2-dimensional faces, creating "short" edges of length 1.

Both models are interesting, although it would seem at first sight that they are dual of one another. This is not quite true, as no transformation can exchange the roles of long and short edges: the short edges indeed interact around the 8 and 4-vertices of the square-diagonal lattice, whereas the long edges do only around the 8-vertices. In the remainder of this section, we will concentrate on the first case, the d-dimensional HCD folding of the 2-dimensional square-diagonal lattice.

6.2. The Model

As in the 2-dimensional case, we choose a particular "fundamental" orientation of the short and long edge "tangent" vectors on both the square-diagonal lattice and the target

d-dimensional HCD lattice, and consider the set of folding configurations of the square-diagonal lattice into the d-dimensional target lattice, namely the set of distinct images of folding maps ρ subject to the constraint (2.2) around each face of the original lattice.

The target short edges may take only $2d$ distinct values, namely $\pm\vec{e_1}$, $\pm\vec{e_2}$, ..., $\pm\vec{e_d}$, where $\vec{e_1}$, ...,$\vec{e_d}$ denotes the orthonormal basis of the d-dimensional hypercubic lattice. The target long edges may take only $2d(d-1)$ distinct values, namely $\pm\vec{e_i}\pm\vec{e_j}$ for $1 \leq i < j \leq d$. The image of a given short tangent vector $\vec{t}$ of the original lattice reads

$$\rho(\vec{t}) \;=\; \epsilon\vec{e_i} \tag{6.1}$$

hence is characterized by a "color" $i \in \{1, 2, ..., d\}$ and a sign $\epsilon = \pm 1$.

In a folding configuration, there are basically only two relative possibilities for the images of the tangent vectors to two adjacent faces sharing a long edge. Indeed, given the values $\vec{u} = \epsilon\vec{e_i}$, $\vec{v} = \eta\vec{e_j}$, $i \neq j$, of the two short edges of the image of the first triangle, there are only two possibilities for the images $\vec{u'}$, $\vec{v'}$ of the two short edges of the second triangle: the face rule (2.2) imposes that $\vec{u'} + \vec{v'} = \vec{u} + \vec{v}$, which holds if and only if

$$\begin{aligned} \vec{u'} = \vec{u} = \epsilon\vec{e_i} \quad &\text{and} \quad \vec{v'} = \vec{v} = \eta\vec{e_j} \\ \text{or} \quad \vec{u'} = \vec{v} = \eta\vec{e_j} \quad &\text{and} \quad \vec{v'} = \vec{u} = \epsilon\vec{e_i} \end{aligned} \tag{6.2}$$

This leaves us again with the only two possibilities of (2.4). As a corollary, the long edge adjacent to the two triangles is always either completely folded, or unfolded.

Let us now investigate the folding configurations of short edges. The two triangles adjacent to a short edge have images of the form

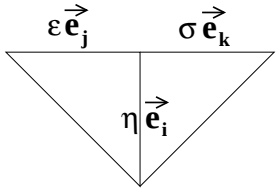

(6.3)

where $i \neq j$ and $i \neq k$.

This gives rise to essentially four types of foldings for the short edge, as depicted in Fig.13. If $j = k$, the short edge is completely folded (180°) when $\sigma = \eta$ and unfolded when $\sigma = -\eta$. If $j \neq k$, the long edge is always folded at a right angle, either up or down according to the relative values of ϵ, σ and η.

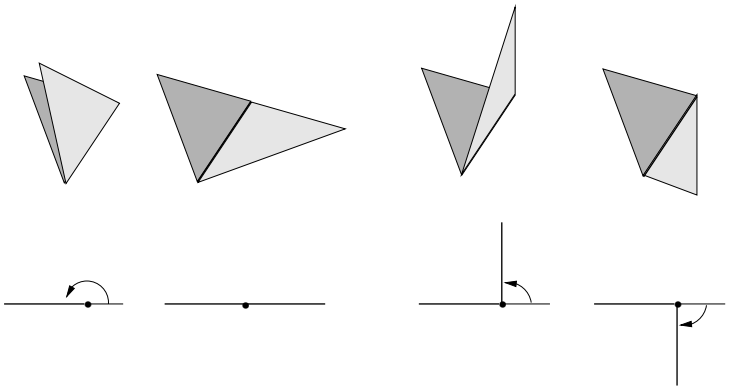

Fig. 13: The four types of folds of the short edge separating two triangles in the d-HCD model: complete fold, no fold, right angle up, right angle down. The figure is drawn in the space spanned by $\vec{e_i}, \vec{e_j}, \vec{e_k}$ of (6.3).

6.3. Equivalent Loop model

The only constraint coming from the face rule (2.2) on a given triangle is that the two short edges should have perpendicular images, of the form $\pm\vec{e_i}$ and $\pm\vec{e_j}$ respectively, with $1 \leq i \neq j \leq d$, namely that they be painted with different colors i and j.

A folding configuration of the square-diagonal lattice in d dimensions amounts to a coloring of all the short edges with colors $i = 1, 2, ..., d$, and a choice of signs $\epsilon = \pm 1$, which propagate along each loop of a given color (according to (6.2)).

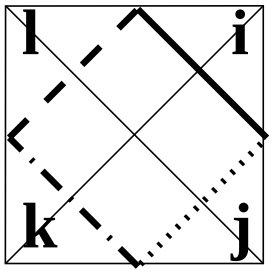

Fig. 14: The "dual" coloring of the faces of S in the d-HCD model. The former short and long edges are represented in thin solid lines. The new edges have the same colors i, j, k, l as the short edges they intersect.

To best see this, let us consider the square-diagonal lattice, together with its square sub-lattice S, whose vertices are those of valency 8 in the original lattice. The lattice S has therefore long edges, and each of its faces is made of 4 former triangles, hence has 4 short edges along its diagonals. Let us replace the coloring of the short edges by that of "dual" edges linking the midpoints of the edges of S around its faces, as illustrated in

Fig.14. Thanks to (6.2), it is now clear that the new colored edges form loops of fixed colors, and that the signs of the tangent vectors (6.1) are constant along those. Note that the coloring of the faces of S must result in the formation of loops of fixed color. This is a constraint on the coloring of the dual edges. Namely, across each long edge separating two adjacent faces of S, the colorings must be either reflected or propagated as follows

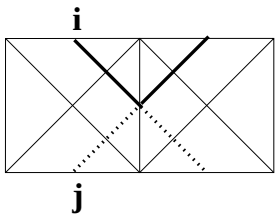

or

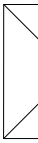

(6.4)

corresponding respectively to the two cases of (6.2).

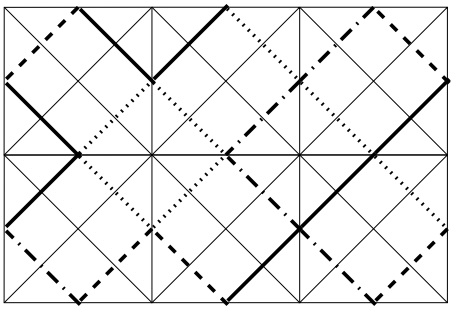

Fig. 15: A sample coloring of S with $d = 4$ distinct colors, represented by solid, dashed, dot-dashed and dotted lines. The original square-diagonal lattice is represented in thin solid lines. Note that the lines are either propagated or reflected according to (6.4) across each long edge. The sign of the image of the short tangent vectors is constant along each line of a given color.

A sample coloring is displayed in Fig.15, with $d = 4$ different colors. Finally, the partition function of the d-dimensional HCD folding of the square-diagonal lattice reads

$$Z_{HCD}^{(d)} = \sum_{\substack{d-\text{colorings} \\ \text{of } S}} 2^{N_1+N_2+\ldots+N_d} \tag{6.5}$$

where the sum extends over all possible colorings with d colors of the faces of S with the gluing constraint (6.4) for adjacent faces. In (6.5), N_i stand for the number of loops of color i, and the factor 2 per loop of a given color accounts for the two possible choices of sign of $\rho(\vec{t})$ (6.1) along that loop. Note that (6.5) reduces to (2.7) when $d = 2$.

6.4. Estimates for the d-HCD Folding Entropy

The expression (6.5) for the partition function of the d-dimensional HCD folding of the square-diagonal lattice provides us with upper and lower bounds on the entropy.

First of all, note that

$$Z_{HCD}^{(d)} \leq Z_{HCD}^{(d+1)} \tag{6.6}$$

as $Z_{HCD}^{(d)}$ is a partial sum of $Z_{HCD}^{(d+1)}$ corresponding to no loop of color $d+1$ ($N_{d+1}=0$). This shows that all the corresponding thermodynamic entropies $s_{HCD}^{(d)}$ are non-zero for $d \geq 2$.

To find a lower bound on $s_{HCD}^{(d)}$, let us try to expand (6.5) around one of its "fundamental" states maximizing the total number of loops $N_1 + ... + N_d = N/4$. Note that there are as many such states as d-colorings of the vertices of S with colors $1, 2, ..., d$ and such that no two adjacent vertices have same color. Indeed, a fundamental state is made of loops of minimal length 4 surrounding each vertex of S such that any two neighboring loops have distinct colors, hence the loop configuration is equivalent to a vertex-coloring. For these fundamental configurations, we have a first rough estimate of $Z_{HCD}^{(d)}$ (actually a lower bound) in the form

$$Z_{HCD}^{(d)} \ \geq \ 2^{N/4} \ Z_S(d) \tag{6.7}$$

where $Z_S(d)$ denotes the number of d-colorings of the vertices of S. This is the leading order of the Mayer expansion of the partition function. The d-coloring entropy $s_S(d) \ = \ \lim_{N\to\infty} \mathrm{Log}(Z_S(d))/N$ is known exactly in the thermodynamic limit only for $d = 2$ and 3. As we already pointed out, there are indeed only two groundstates at $d = 2$, i.e. $Z_S(2) = 2$, and the thermodynamic entropy per site is $s_S(2) = 0$: (6.7) then leads to (2.9). For $d = 3$, the 3-coloring problem of the vertices of the square lattice S (or equivalently of the faces of its dual S^*) is equivalent to the ice model [12], with an entropy per site

$$s_S(3) \ = \ \frac{3}{2}\mathrm{Log}(\frac{4}{3}) \tag{6.8}$$

This gives the lower bound for $d = 3$

$$s_{HCD}^{(3)} \geq \frac{1}{4}\mathrm{Log}\,2 + \frac{1}{4}s_S(3) \ = \ \mathrm{Log}\,2 - \frac{3}{8}\mathrm{Log}\,3 \ = \ .281167... \tag{6.9}$$

or a partition function per triangle of 1.32467...

Let us estimate the lower bound (6.7) when d is large. As a very rough leading approximation, each vertex of S can be painted with one of d colors, minus the small

number of colors used for its neighbouring vertices, hence if d is very large, we have $Z_S(d) \simeq d^{N/4}$. This gives the leading estimate

$$s_{HCD}^{(d)} \;\simeq\; \frac{1}{4}\mathrm{Log}(2d) \tag{6.10}$$

A more careful study shows that this is accurate up to the order of $1/d$.

6.5. Vertex Model

As in the $d = 2$ case, let us transform the colored loop model of Sect.6.3 into a vertex model, by mapping the coloring configurations and sign choices on each face of S onto Vertex configurations for the dual square lattice S^*. Each colored new edge on the faces of S has been assigned a color $i \in \{1, 2, ..., d\}$ and a sign $\epsilon \in \{-1, 1\}$ (see Fig.14), which are conserved (either propagated or reflected, according to (6.4)) at each crossing of an edge of S. This suggests to attach to each edge of S^* a *pair* of colors and signs $(i, \sigma; j, \tau)$, with say $1 \leq i < j \leq d$. This gives $2d(d-1)$ possible values for this edge variable. The vertex model is then defined by the list of all possible edge configurations around a vertex of S^*, together with the gluing property that each edge of S^* has a well-defined configuration. Each allowed vertex has Boltzmann weight 1.

Let us count the number of allowed vertices for generic values of d. This is the same as the number of coloring and sign configurations on each face of S. To count the latter, note that the only constraint on the four color/sign pairs $(i_1, \sigma_1), ..., (i_4, \sigma_4)$ is that any two consecutive colors must be distinct. So we merely have to count the number of cyclic arrangements of four colors taken among d around the face. Introducing the $d \times d$ matrices I and J, with entries $I_{i,j} = \delta_{i,j}$, and $J_{i,j} = 1$ for all i, j, the total number of vertices reads

$$V_d \;=\; 16\mathrm{Tr}(J - I)^4 \;=\; 16d(d-1)(d^2 - 3d + 3) \tag{6.11}$$

where we have used the relation $J^2 = dJ$, and factored out the contribution 16 for the independent choices of the four signs.

Note that (6.11) yields $V_2 = 32$ instead of 28, for $d = 2$. This is because we must keep track of the edge colors as soon as $d > 2$. At $d = 2$, the model has been further simplified by noticing that any reference to the edge coloring could be omitted, at the expense of modifying the Boltzmann weights (four vertices actually acquired a Boltzmann weight 2).

The row-to-row transfer matrix of the vertex model is again sparse. Indeed, if we fix the value of the west-most edge in a row of N vertices, we have a number of non-vanishing matrix elements of the order of $(V_d/(2d(d-1)))^N$, whereas the matrix has a total of $(2d(d-1))^{2N}$ elements, hence a ratio $[2(d^2 - 3d + 3)/(d^2(d-1)^2)]^N$, which gets smaller as d increases.

6.6. Numerical Study

In this section, we extract some numerical estimates for the HCD folding entropy in dimension $d = 3$, from the largest eigenvalue of the transfer matrix of the 288 Vertex model described in the previous section.

n	λ_{max}	ν_n
1	2.000000	
2	5.587741	1.29286
3	17.11799	1.32298
4	54.54084	1.33603
5	177.4631	1.34306

Table IV: Numerical results for the transfer matrix of the $V_3 = 288$ Vertex model with fixed boundary conditions ($=(1, +; 2, +)$ on both ends) for the 3-dimensional HCD folding. We have represented the size n of the row, the largest eigenvalue and the ratio $\nu_n = (\lambda_{n+1}/\lambda_n)^{1/4}$, which converges to the partition function per triangle.

We are indeed limited by the rapid growth of the size of the transfer matrix, and more importantly of its number of non-vanishing entries, which grows like $(8(d^2 - 3d + 3))^n$ for a row of width n. At $d = 3$, this is already 24^n, and we have been only able to consider transfer matrices up to the width $n = 5$, with fixed boundary conditions (with the edge variables fixed to $(i, \sigma; j, \tau) = (1, +; 2, +)$ on both ends).

The results for the largest eigenvalue of the corresponding transfer matrix of the 288 Vertex model are displayed in Table IV, together with the sequence $\nu_n = (\lambda_{max}(n + 1)/\lambda_{max}(n))^{1/(4n)}$, converging to the partition function per triangle $z^{(3)}_{HCD}$. The extrapolated thermodynamic entropy reads

$$s^{(3)}_{HCD} \simeq .300.. \tag{6.12}$$

or a partition function per triangle $z^{(3)}_{HCD} \simeq 1.35(1)$ Note that our estimate (6.12) agrees with the lower bound (6.9).

7. d-Dimensional FCH Folding

7.1. The Model

As in the 2-dimensional case, we choose a particular "fundamental" orientation of the short and long edge "tangent" vectors of the d-HCD lattice of Fig.12, and consider the set

of folding configurations of the square-diagonal lattice into the d-dimensional FCH lattice, namely the set of distinct images of folding maps ρ subject to the constraint (2.2) around each face of the original lattice.

The target long edges may take only $2d$ distinct values, namely $\pm\vec{f}_1$, $\pm\vec{f}_2$, ..., $\pm\vec{f}_d$, where $\vec{f}_1$, ...,$\vec{f}_d$ form an orthogonal basis of $\mathbb{R}^d$ (with $|\vec{f}_i| = \sqrt{2}$ for all i). The target short edges may take only $2d(d-1)$ distinct values, namely the unit vectors $(\pm\vec{f}_i \pm \vec{f}_j)/2$ for $1 \le i < j \le d$.

In a folding configuration, there are many possibilities for the images of the tangent vectors to two adjacent faces sharing a long edge, namely

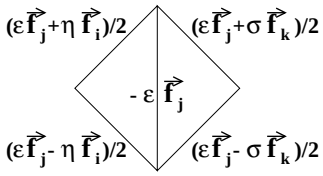

(7.1)

where $i, j, k \in \{1, 2, ..., d\}$, i and k distinct from j, and ϵ, η, σ are arbitrary signs.

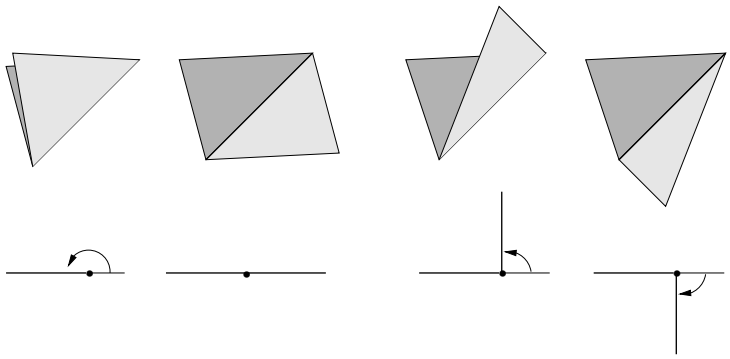

Fig. 16: The four types of folds of the long edge separating two triangles in the d-FCH model: complete fold, no fold, right angle up, right angle down. The figure is drawn in the space spanned by $\vec{f}_i, \vec{f}_j, \vec{f}_k$ of (7.1).

This gives rise to essentially four types of foldings for the long edge, as depicted in Fig.16. If $i = k$, the long edge is completely folded (180°) when $\sigma = \eta$ and unfolded when $\sigma = -\eta$. If $i \neq k$, the long edge is always folded at a right angle, either up when $\sigma = \eta$ (+90°), or down if $\sigma = -\eta$ (−90°).

7.2. Vertex Model

Let us again consider the square lattice S whose vertices are the 8-valent vertices of the square-diagonal lattice. The edges of S are the long edges of the original lattice.

According to the previous section, these edges are folded into edges of the form

$$\rho(\vec{t}) \;=\; \epsilon \vec{f}_i \tag{7.2}$$

Each such image is therefore characterized by a color $i \in \{1, 2, ..., d\}$ and a sign $\epsilon \in \{-1, 1\}$. Let us examine the possible relative images of the long edges in two triangles sharing a short edge. There are basically only two possibilities

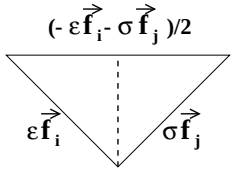

or

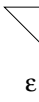

(7.3)

to accomodate the face rule (2.2), where $i \neq j$, $i \neq k$, and ϵ, σ, η are arbitrary signs. We have indicated only the value of the central short edge image, as the remaining ones are immediately deduced from the face rule (2.2). As a corollary, we see that the short edges are always either completely folded (solid line in (7.3)), or unfolded (dashed line in (7.3)). Together with Fig.16, this shows a complete parallel between the d-HCD and d-FCH models: we see that the roles of the long and short edges are exchanged in the two models, at least as far as the types of folding are concerned. Note however that there are twice as many short edges as long edges in the square-diagonal lattice, we therefore expect a difference in the folding entropies of the two models.

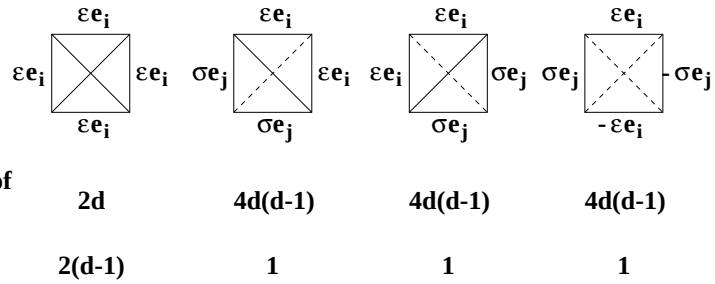

Fig. 17: The allowed configurations of long edges around a face of S in the d-FCH model. We have indicated the degeneracy of each face configuration and the corresponding Boltzmann weight. The inner short lines represent the state of the corresponding short edges, namely completely folded (solid line) or unfolded (dashed line).

Let us now investigate the possible configurations of the images of the long edges around a face of S. Using (7.3) and proceeding by inspection, we have found the face configurations displayed in Fig.17, together with their degeneracy and attached Boltzmann

weight. From (7.3), we find a unique image for each internal short edge in the three last cases of Fig.17 (hence a weight 1), whereas in the first case much freedom is left: indeed, the inner edge images may take values $(-\vec{f}_i \pm \vec{f}_k)/2$, for any value of $k \neq i$, the same for all edges, and with alternating signs as we move around the face. This results in $2 \times (d-1)$ possible inner values, hence the corresponding Boltzmann weight of Fig.17. Let us count these allowed configurations. From Fig.17, we count

$$W_d \;=\; 2d + 3 \times 4d(d-1) \;=\; 2d(6d-5) \tag{7.4}$$

distinct vertices.

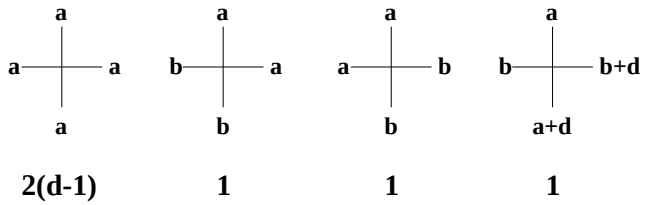

Fig. 18: The allowed vertices of the W_d Vertex model, with the corresponding Boltzmann weight. The edge variable is defined modulo $2d$ and we have $a \neq b \bmod d$.

The face configurations of Fig.17 may be recast into the vertex configurations of Fig.18 of the dual square lattice S^*, in which each edge is assigned an image $a \in \mathbb{Z}_{2d}$, with the correspondence

$$(+, \vec{f}_i) \;\rightarrow\; a = i-1 \qquad \text{and} \qquad (-, \vec{f}_i) \;\rightarrow\; a = d+i-1 \tag{7.5}$$

for $i = 1, 2, ..., d$.

When $d = 2$ we recover the $W_2 = 28$ Vertex model, with the correct assignments of Boltzmann weights of Fig.10, up to the correspondence (7.5) between the edge variables. This shows how our two (d-HCD and d-FCH) d-dimensional foldings agree with the unique model for $d = 2$ in quite different ways, providing for two different points of view on the $d = 2$ model. We will elaborate on this in a later section.

The present W_d Vertex model appears to be much simpler than the V_d Vertex model for the d-HCD folding. Indeed, the edge variables may take only $2d$ values (to be compared to the $2d(d-1)$ values in the other model), and the number of distinct vertices (7.4) is only a quadratic polynomial of d (to be compared with the quartic polynomial (6.11)). The only price to pay for this simplification is the Boltzmann weight $2(d-1)$ for completely folded faces.

The transfer matrix for the W_d Vertex model is again sparse, with a ratio $[(6d-5)/(4d^2)]^N$ of non-vanishing elements. It gives easier access to numerical calculations, at least for small enough values of d.

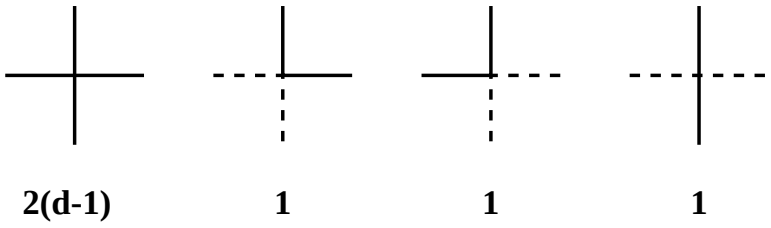

Fig. 19: The four types of colored vertices for the d-FCH folding model. The solid and dashed lines stand for any two distinct colors in $\{1, 2, ..., d\}$. The signs are conserved along colored lines, except for the last vertex, where they are reversed.

7.3. Loop Model

The W_d Vertex model of the previous section can be refined as follows. Let us disentangle the sign and color variables on each edge of S^*, and represent only the color of the edge, by painting it accordingly. This leaves us with only the four types of vertices depicted in Fig.19. the signs must now be conserved or reversed along colored lines according to Fig.17. The sign is actually conserved in all cases, except when the two lines of different color cross each other (last, completely unfolded case of Fig.17), in which case it is reversed. These colored lines form loop-like clusters, along which the signs are entirely determined by their value on one of the edges of the cluster. Moreover, all values are compatible, as there are always an even number of sign reversals (due to an even number of crossings with lines of other colors) along a loop.

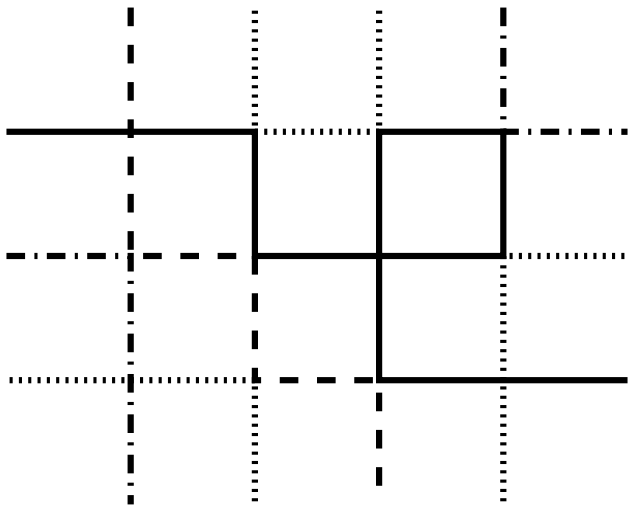

Fig. 20: A sample coloring configuration for the d-FCH folding model, for $d = 4$.

Hence on top of the Boltzmann weights indicated in Fig.19, we must include a weight 2 per loop-like cluster of given color. A sample configuration of the model for $d = 4$ is displayed in Fig.20 for illustration. With free boundary conditions, this configuration would receive the weight $2^7 \times 2(4-1) = 1536$, as 7 colored clusters are formed, and one vertex is of the first type of Fig.19.

7.4. Estimates for the d-FCH Folding Entropy

The loop model of previous section permits to derive lower bounds on the partition function $Z_{FCH}^{(d)}$ of the d-FCH folding model, henceforth on the d-FCH folding entropy.

We first note that there are exactly $2d$ fundamental configurations of the loop model with minimum energy (i.e. maximum Boltzmann weight), namely those obtained with only the first vertex of Fig.18, that is where all the edges are painted with the same color. The contribution to the partition function of each of these groundstates is $[2(d-1)]^n$ for a portion of S^* with n vertices. Using Fig.17, these correspond to completely folded configurations of all the short edges.

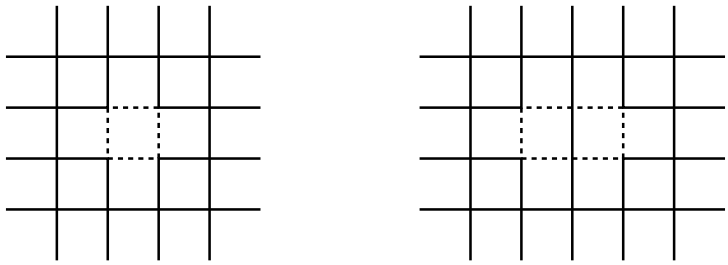

(a) **(b)**

Fig. 21: A few local excitations of the all-black groundstate of the W_d Vertex model. We have represented a single excitation (a), formed by a loop of any of the $(d-1)$ other colors and a pair of neighboring excitations (b) with necessarily identical colors. The single excitation (a) suppresses 4 black vertices of the groundstate, whereas the pair suppresses 6 of them.

Let us fix such a groundstate, say of color 1 (black). Consider the local excitation obtained by forming a minimal loop of another color, as depicted in Fig.21(a). The loop suppresses 4 vertices of the first type in Fig.19, but introduces an extra weight $2(d-1)$ for the extra loop and the choice of $d-1$ other colors to paint it. Hence the local excitation contributes an overall relative weight of $1/(2(d-1))^3$. These excitations do interact whenever they occupy neighboring faces of S^*. For instance, as shown in Fig.21(b),

two such neighboring excitations are forced to have the same color, and form only one extra loop, whereas they suppress 6 vertices of the first type in Fig.19. Hence, instead of the expected relative weight $1/(2(d-1))^6$, they only contribute for $(2(d-1))/(2(d-1))^6 = 1/(2(d-1))^5$. This propagates to higher numbers of excitations. In general, the partition function is underestimated if we neglect these interactions. This provides us with an exact lower bound

$$Z_{FCH}^{(d)} \ \geq \ \left[2(d-1)(1+\frac{1}{(2(d-1))^3})\right]^n \tag{7.6}$$

hence

$$s_{FCH}^{(d)} \ \geq \ \frac{1}{4}\mathrm{Log}\left(2(d-1)(1+\frac{1}{(2(d-1))^3})\right) \tag{7.7}$$

d	entropy	p. func.
2	.20273255	1.224744
3	.35044964	1.419705
4	.44909460	1.566892
5	.52034819	1.682613
6	.57589615	1.778723
7	.62137130	1.861478
8	.65985542	1.934512
9	.69320821	2.000122
10	.72263580	2.059855

Table V: Lower bound on the d-dimensional FCH folding entropy, from (7.7). We display the dimension d, the lower bound on the folding entropy and the corresponding lower bound on the partition function per triangle.

The values of the lower bound (7.7) for the d-FCH model are displayed in Table V. Note that (7.7) consists of the two leading orders of the Mayer expansion of $Z_{FCH}^{(d)}$ in terms of the local excitations described above. The expansion however is quite involved, as the excitations interact between nearest neighbours (two faces sharing an edge) and second-nearest neighbors (two faces sharing a vertex) as well. In the latter case, we have to use extra caution and distinguish between the cases when the two excitations have the same or different colors. Up to order 2 in these excitations, we find

$$\left(Z_{FCH}^{(d)}\right)^{\frac{1}{n}} \ = \ u(1+\frac{1}{u^3}+\frac{5}{u^5}-\frac{8}{u^6}+O(\frac{1}{u^7})) \tag{7.8}$$

where we have set $u = 2(d-1)$. Note the bad apparent convergence at $d = 2$ ($u = 2$), where this yields $z \simeq 1.233$, way below our best estimate 1.258. It appears that for $d = 2$ the Mayer expansion (2.13) around a very different groundstate is much more accurate. So, although both have the same contribution 2^n to the partition function, the latter groundstate yields better corrections. This competition between different groundstates could yield an interesting phase diagram for a fully interacting model.

We expect however the expansion (7.8) to behave better for larger values of d, for which the existence of a groundstate generalizing that leading to (2.13) is not clear.

Comparing (7.7) to the large d estimate (6.10) for the HCD model, we conclude that the two d-dimensional folding models (HCD and FCH) agree in the large d limit.

7.5. Numerical Study

In view of the previous sections, the W_d Vertex model is a straightforward generalization of the 28 Vertex model we have already studied. A direct adaptation of our programs permits to calculate the largest eigenvalue of the transfer matrix for a few values of d.

Like in the $d = 2$ case, we use the method of iteration of the action of the transfer matrix T on a given vector, which we normalize at each step. To construct T, we simply list its $(6d-5)^n$ non-zero elements, for fixed boundary conditions (say $= 0$) on the leftmost edge of the row. Each such element has a unique pair of (row,column) indices in T: indeed, the type of vertex in Fig.18 is fixed uniquely whenever the east, north and south edge variables are given. Like in the $d = 2$ case, this linear description of the matrix gives access to large sizes. We list our results in Table VI below, for fixed boundary conditions ($= 0$) on both ends.

	n $\lambda_{\max}$ ν_n		n $\lambda_{\max}$ ν_n
	1 4.0000000		1 6.0000000
$d = 3$	2 16.271109 1.420166	$d = 4$	2 36.170708 1.566936
	3 67.253188 1.425850		3 218.18854 1.567179
$W_3 = 78$	4 280.96435 1.429666	$W_4 = 152$	4 1316.2983 1.567222
	5 1185.8001 1.433309		5 7941.2213 1.567231
	6 5063.2725 1.437490		
	1 8.0000000		1 10.000000
$d = 5$	2 64.127762 1.682631	$d = 6$	2 100.10133 1.778729
	3 514.66822 1.683140		3 1002.5120 1.778944
$W_5 = 250$	4 4131.2200 1.683207	$W_6 = 372$	4 10040.689 1.778969
	5 33162.598 1.683226		

Table VI: Numerical results for the transfer matrix of the W_d Vertex model with fixed boundary conditions (= 0 on both ends). We list the dimension d, the length n of the row, the largest eigenvalue $\lambda_{\max}$, and the sequence $\lambda_{\max}^{1/(4n)}$, and $\nu_n = (\lambda_{n+1}/\lambda_n)^{1/4}$, converging to the partition function per triangle.

These values are extrapolated to the following

$$\begin{array}{llll} s_{FCH}^{(3)} & = .378... & z_{FCH}^{(3)} & = 1.47... \\ s_{FCH}^{(4)} & = .4493... & z_{FCH}^{(4)} & = 1.5672... \\ s_{FCH}^{(5)} & = .5207... & z_{FCH}^{(5)} & = 1.6832... \\ s_{FCH}^{(6)} & = .57603... & z_{FCH}^{(6)} & = 1.77896... \end{array} \tag{7.9}$$

for the entropy s_{FCH} and the partition function per triangle z_{FCH}. Note the excellent agreement with the lower bounds of Table V, for $d = 4, 5, 6$. We expect the Mayer expansion (7.8) to be an excellent approximation to the partition function per site for all $d \geq 4$.

n	λ_{max}	ν_n
1	5.000000	
2	24.21917	1.48353
3	119.4202	1.49014
4	582.3144	1.48600
5	2812.592	1.48247
6	13498.13	1.48010

Table VII: Numerical results for the transfer matrix of the W_3 Vertex model with mixed boundary conditions (= 0 on one end, free on the other) for the 3-dimensional FCH folding. We have represented the size n of the row, the largest eigenvalue and the ratio $\nu_n = (\lambda_{n+1}/\lambda_n)^{1/4}$, which converges to the partition function per triangle.

For $d = 3$, we observe a much slower convergence (see Table VI). To obtain better results, we have also calculated the largest eigenvalue of the transfer matrix T in the case of mixed boundary conditions, fixed at 0 on one end, and free on the other. The results are displayed in Table VII. Upon extrapolation, this leads to a more precise result for the 3-dimensional FCH folding entropy and partition function per triangle:

$$s^{(3)}_{FCH} \simeq .3854... \qquad z^{(3)}_{FCH} \simeq 1.470.. \tag{7.10}$$

8. Other Compactly Foldable Lattices

8.1. Classification of Compactly Foldable Lattices

We would like to briefly address the following question: can one classify the inequivalent two-dimensional lattices which are compactly foldable onto themselves in two dimensions? By this we mean that all maps ρ preserving the face rule (2.2) and the lengths of edges, and with values in $\mathbb{R}^2$ actually have their image included in the original lattice. Another formulation is the existence of a map ρ whose image is a single face of the lattice (the lattice is then completely foldable onto that face).

We already know of three examples: the square lattice (and its trivial variation the rectangular lattice), the regular triangular lattice and the square-diagonal lattice introduced in this paper.

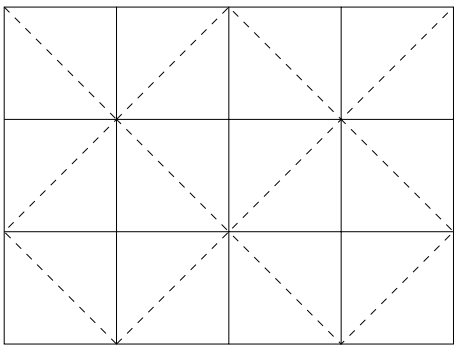

Fig. 22: The square-diagonal lattice as the superposition of two square lattices S and S'. The edges of S are represented in solid lines, those of S' in dashed lines.

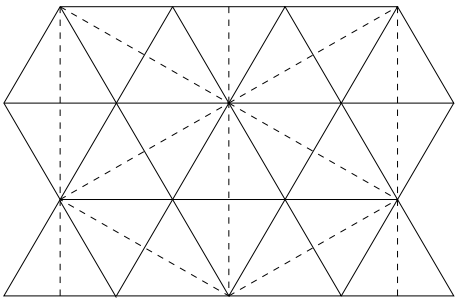

Fig. 23: The dilation/rotation transformation on the triangular lattice gives rise to another triangular lattice represented in dashed lines. The superposition of the two forms a new foldable lattice, with long, medium and short edges.

One way to look at the square-diagonal lattice is rather as the superposition of two square lattices (see Fig.22), say S and S', such that S' is a dilated version of S by a factor $\sqrt{2}$ as well as rotated by 45°, so that the vertices of S' coincide with half of the vertices of S, forming a checkerboard.

This suggests to apply the same type of transformation (dilation/rotation) to the triangular lattice. The only non-trivial possibility is a dilation by a factor of $\sqrt{3}$, and a rotation by 30°, displayed in Fig.23. This gives rise to a new foldable lattice in two dimensions, by superposition of the two triangular lattices, called the double-triangular lattice. We expect its entropy of two-dimensional folding to be larger than that of the square-diagonal model. This model will be studied in the next section.

This can be shown to actually exhaust all the possibilities for compactly foldable two-dimensional lattices. As a side remark, the generating function for compactly foldable random triangulations of arbitrary genus was obtained in [13].

8.2. Two-Dimensional Folding of the Double-Triangular Lattice

The double-triangular lattice of Fig.23 has three types of edges: long, medium, short of respective lengths 2, $\sqrt{3}$, 1. Each triangular face has one edge of each type. As usual, we introduce tangent vectors along these edges, with compatible orientations throughout the lattice, so that the face rule (2.1) is satisfied around each triangular face.

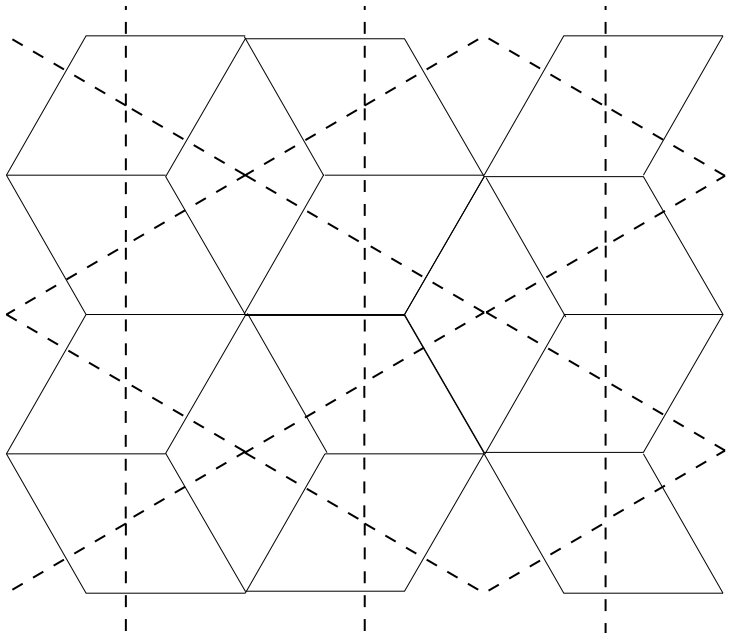

Fig. 24: The diamond lattice formed by the long edges of the double-triangular lattice (solid lines), and its dual, the Kagomé lattice (dashed lines).

A folding configuration of the lattice is a continuous map ρ of these tangent vectors to the plane, such that the face rule (2.2) is satisfied around each elementary triangular face. Let us now first concentrate on the long edges of the double-triangular lattice. They form the diamond-lattice, represented in solid lines in Fig.24, which is dual to the Kagomé lattice, represented in dashed lines in the same figure.

By inspection, it is easy to see that the images of the long edge vectors may only take one of the six values $\pm\vec{e_1}$, $\pm\vec{e_2}$, $\pm\vec{e_3}$, where the $\vec{e_i}$ are three fixed vectors of length 2 with vanishing sum (hence forming angles of 120°). As before, writing these images as

$$\rho(\vec{t}) \;=\; \epsilon\vec{e_i} \tag{8.1}$$

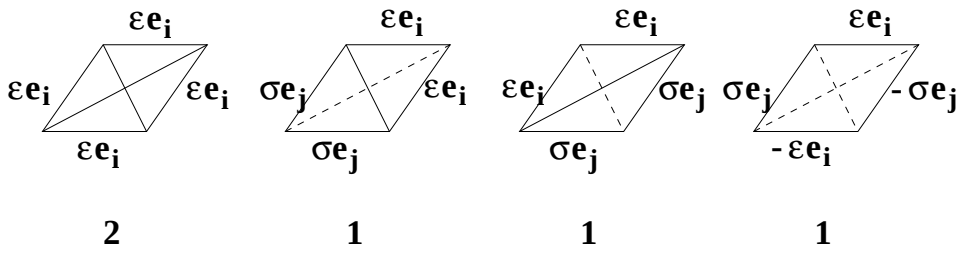

Fig. 25: The four possible configurations of long edges around a diamond-shaped face. We have represented in dashed lines the (medium or short) unfolded inner edges, and in solid lines the folded inner edges. We have also indicated the attached Boltzmann weights. The color indices take the values $i, j = 1, 2, 3$, with $i \neq j$, and ϵ, σ are arbitrary signs.

this suggests to attach a color $i = 1, 2, 3$ to each long edge, and a sign $\epsilon = \pm 1$.

In a way very similar to the square-diagonal case, the long edges around any diamond-shaped face of Fig.24 may only take the four possible relative values depicted in Fig.25, according to the folding state of the inner short and medium edges. Note the Boltzmann weights, 1 for the last three cases of Fig.25, as the inner edges are entirely fixed, and 2 for the first case, as we have two choices for the inner short edges $\vec{s} = \epsilon \vec{e_k}/2$, $k \neq i$, which then fix all other inner edges. Each long edge may take 6 values. This gives a total of 78 distinct possible diamond face environments. These turn out to be in one-to-one correspondence with the 78 cases of Fig.17, when $d = 3$, but with different Boltzmann weights. This gives a remarkable relation between a two-dimensional folding problem and a three-dimensional one.

Like in the d-FCH folding case, we may now rephrase the folding problem as a 78 Vertex model on the edges of the dual Kagomé lattice of Fig.24, in which each edge may take a value $a \in \mathbb{Z}_6$, and with the vertices derived from Fig.25. The transformation into a colored cluster model performed in Sect.7.3 is still valid here. Hence the model is equivalent to a colored cluster model with the vertices of Fig.26, similar to that of Fig.19, with 3 edge colors, and with a weight 2 per vertex of the first type, and an extra Boltzmann weight of 2 per cluster. Note that the three different types of vertices of the Kagomé lattice are not distinguished in the present model.

This permits to derive a simple lower bound on the two-dimensional folding entropy s_{DT} of the double-triangular lattice. Indeed, let us start from one of the 3 groundstates of the vertex model, in which all the edges are painted with the same color. There are $N/4$ such vertices, corresponding to $N/4$ diamond faces in the dual, each of which contains 4 triangles, for a total number of N triangles. We therefore obtain the lower bound

$$Z_{DT} \;\geq\; 2^{N/4} \tag{8.2}$$

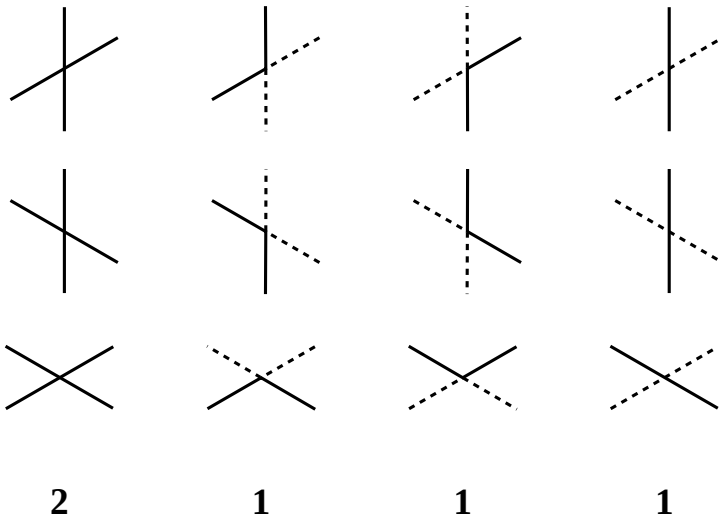

Fig. 26: The allowed vertices of the tri-colored cluster model on the Kagomé lattice, equivalent to the two-dimensional DT folding problem. The solid and dashed lines stand for any two distinct colors among $\{1, 2, 3\}$. We have indicated the Boltzmann weight under the three corresponding vertices. Each colored cluster has a fugacity 2.

for the partition function of the two-dimensional double-triangular lattice model.

This can be easily improved by considering the local excitations of Sect.7.4. In the present case, these correspond to creating a minimal triangular loop of one of the two other colors than that of the groundstate. Such a loop suppresses 3 vertices of weight 2 each, and contributes for an extra weight 2 for the two choices of color, and the weight 2 for the loop created. Each such local excitation contributes therefore a relative weight $4/2^3 = 1/2$ to the partition function. As before, neglecting the contact interactions between these excitations, we get an exact lower bound for the partition function

$$Z_{DT} \;\geq\; 2^{N/4}(1+\frac{1}{2})^{N/6} \tag{8.3}$$

where we have identified the total number $N/6$ of excitable triangles. This gives the lower bound

$$s_{DT} \;\geq\; \frac{1}{4}\mathrm{Log}\,2 + \frac{1}{6}\mathrm{Log}\big(1+\frac{1}{2}\big) \;=\; .2408... \tag{8.4}$$

or a partition function per triangle of at least 1.2723...

Two excitations sharing a vertex interact as follows. If the two excited triangles have the same color, they receive a weight 2 for the choice of color, 2 for the cluster formed, and 5 black vertices are erased, but one of the other color is created, hence a total contribution $2 \times 2/2^4 = 1/4$. If their colors are distinct, they receive a weight 2 for the choices of this

pair of colors, 2×2 for the two created loops, and 5 black vertices are suppressed, hence a total weight $2^3/2^5 = 1/4$. Two neighboring excitations therefore contribute a total of $1/4 + 1/4 = 1/2$ instead of the expected $1/4$. These may take any of the $N/4$ positions available for their common vertex on the Kagomé lattice. Up to two excitations, the Mayer expansion of the folding entropy therefore reads

$$s_{DT} \;\simeq\; \frac{1}{4}\mathrm{Log}\,2 + \frac{1}{6}\mathrm{Log}\big(1 + \frac{1}{2} + \frac{3}{8}\big) \;=\; .278... \tag{8.5}$$

or a partition function per triangle $z_{DT} \simeq 1.320....$

8.3. d-dimensional Folding of the Double-Triangular Lattice

We now briefly address the question of the d-dimensional foldings of the double-triangular lattice.

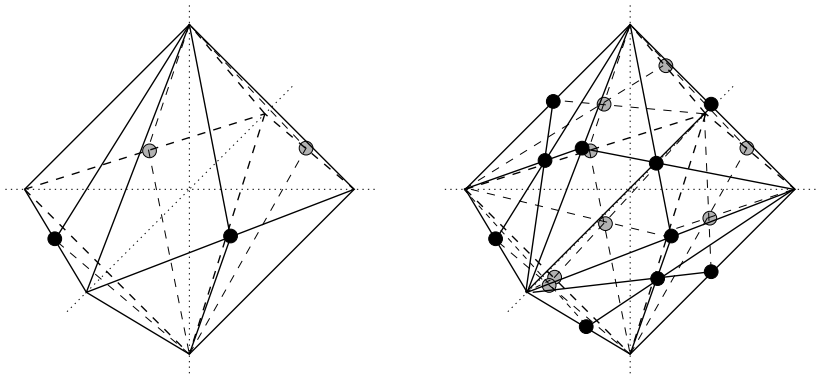

(a) **(b)**

Fig. 27: The unit cells of the two possible 3-dimensional lattices onto which that of Fig.23 can be folded. Both are decorations of the 3-dimensional FCC lattice, whose unit cell is an octahedron. We have represented the vertices added to the original FCC unit cell by filled dots.

The reader will convince himself that there are again two possibilities here, according to whether we privilege long or short edges. The first possibility consists in starting from the d-dimensional FCC lattice of [10], whose unit cell is made of a polytope, with $2d$ vertices at the points $(0, 0, .., 0, \pm 1, 0, .., 0)$ in $\mathbb{R}^d$, with edges joining any pair of these points with non-zero coordinate in different places, and regular triangular faces joining any triple of such points. Next we introduce new vertices in the middle of one third of all edges, which we join to the opposite vertices of all faces adjacent to that edge, thus constructing exactly

one height on each triangle. We do this in a coherent way, by successively sending the height from a triangle to its neighbors by rotating it around any of the two opposite edges of its face. In the end, each section of the lattice by a plane containing one of its faces must be the lattice of Fig.23. The octahedral unit cell of the 3-dimensional version is represented in Fig.27(a).

The other possibility also starts from the d-dimensional FCC lattice. We next simply add a central vertex in the middle of each face and of each edge, and join them by drawing the three heights of each triangular face of the FCC lattice. The unit cell of this lattice is represented in Fig.27(b) for $d = 3$.

Note that the heights in these two constructions play exactly the role of the diagonals in the case of the square-diagonal lattice folding. Both models lead naturally to higher vertex models on the Kagomé lattice.

9. Discussion and Conclusion

9.1. Folding Entropies

In this paper, we have found various estimates for the entropy of folding of the square-diagonal lattice into target spaces of various dimensions. Let us compare the results we have obtained to another folding problem, that of the triangular lattice in two and three dimensions [4] [10].

In two dimensions, the partition function per triangle for the folding of the triangular lattice was obtained in [4], with the exact result

$$z_T^{(2)} \;=\; \frac{\sqrt{3}}{2\pi}\Gamma(1/3)^{3/2} \;=\; 1.20872... \tag{9.1}$$

The square-diagonal folding partition function per triangle

$$z_{SD} \;=\; 1.2586... \tag{9.2}$$

is substantially larger. In addition, our model presents two different types of edges, to which we can attach different bending energies. Doing so should produce an interesting phase diagram and hopefully confirm the first order folding transition of [9]. The double-triangular folding partition function per triangle

$$z_{DT} \;\simeq\; 1.32... \tag{9.3}$$

is even larger, as expected.

In three dimensions, the best numerical estimate of [10] for the partition function per triangle of the triangular lattice folding reads

$$z_T^{(3)} \;=\; 1.43(1) \tag{9.4}$$

Our present estimates

$$\begin{aligned} z_{HCD}^{(3)} &= 1.35(1) \\ z_{FCH}^{(3)} &= 1.470(1) \end{aligned} \tag{9.5}$$

lie on both sides of (9.4). The main advantage of the FCH folding model is that it deals with much smaller transfer matrices, allowing in principle for better estimates. Again, the introduction of bending rigidity (in the form of a bending energy, e.g.) should lead to an interesting phase diagram. Eq.(9.5) is evidence of the difference between the two (HCD and FCH) 3 dimensional foldings of the square-diagonal lattice. However, we also noted that the two models should agree better and better as d increases.

A last remark is in order, regarding the relation between the d-dimensional HCD and FCH models. Let us consider the following restriction of the W_d Vertex model for the d-FCH model (called rFCH model), in which the first vertex of Fig.18 is assigned a weight 0. This forbids the formation of colored clusters, by suppressing the first vertex of Fig.19. We are therefore left with a model of colored lines, with colors $i = 1, 2, ..., d$, which either avoid (by being reflected) or cross each other on the vertices of S^*, according to whether we have the second, third or fourth vertex of Fig.19. This is therefore a model of dense colored loops, each affected with a weight 2 (for the two choices of signs along each loop). Its partition function reads

$$Z_{rFCH}^{(d)} \;=\; \sum_{\substack{\text{dense colored} \\ \text{loops}}} 2^{N_1+N_2+...+N_d} \tag{9.6}$$

This is strongly reminding of the partition function for the d-HCD model (6.5). Note however two discrepancies. Firstly the coloring rules are different. Although the gluing rules along the edges of the squares in the d-HCD model (6.4) are the same as the vertex rules in the rFCH model (crossing or reflection), they do not take place on the same sites (vertex v/s mid-point of edge). This is probably not a very important difference. The main one is that there are $N/4$ vertices in the rFCH model (for N triangles), and $N/2$ edges in the d-HCD model. So even if the partition functions were identical, we would get

$s^{(d)}_{rFCH} = s^{(d)}_{HCD}/2$ in the thermodynamic limit. From (9.5), we see then that when $d = 3$ only a small portion of the FCH entropy is taken care of by the restricted model. Note finally that the restriction imposes that *at most* one set of two parallel short edges can be folded on each face of S: this rigidifies the faces of S only partially, and the latter can be thought of as a random distribution of exactly one diagonal on each face of a square lattice S, each of which is either folded or not, hence this looks like a randomized version of the square-diagonal lattice, in which the former long edges play the role of short edges, and pairs of parallel former short edges play the role of long edges.

9.2. Bending Rigidity

A natural extension of our models would be the introduction of a bending rigidity, namely of an energy making folding more or less difficult.

In the two-dimensional Square-Diagonal folding problem, this can be implemented by attaching a Boltzmann weight e^{K_i}, per unfolded long ($i = 1$) or short ($i = 2$) edge, while completely folded edges receive weights e^{-K_i} respectively. Positive values of K_i will favor a completely flat groundstate, whereas negative values of K_i will favor a completely folded groundstate.

Interestingly, if we choose $K_1 << 0$ and $K_2 = 0$, the system will tend to maximize its number of folded long edges. This corresponds to either of the two groundstates of Sect.2.3 which have led us to (2.10), with a free energy

$$-\frac{f_{-0}}{kT} \;=\; -\frac{K_1}{2} + \frac{1}{4}\mathrm{Log}2 \tag{9.7}$$

per triangle (there are $N/2$ long edges for N triangles).

If instead we choose $K_1 = 0$ and $K_2 << 0$, the system will have a tendency to have all its short edges folded, hence, in terms of the $W_2 = 28$ Vertex model, the first vertex of Fig.10 will be favored, namely all edges will have the same value of a. The corresponding four groundstates are those of Sect.7.4 which have led us to (7.6), for $d = 2$. The corresponding free energy per triangle reads

$$-\frac{f_{0-}}{kT} \;=\; -K_2 + \frac{1}{4}\mathrm{Log}2 \tag{9.8}$$

(there are N short edges for N triangles).

More generally, the situation $K_2 = 0$, K_1 arbitrary can still be described within the framework of the 28 Vertex model of Fig.10. Indeed, the first vertex receives a Boltzmann

weight $2e^{-4K_2}$ (all four inner short edges are folded), the last one a weight e^{4K_2} (all four inner short edges are flat) and the two remaining vertices receive a weight 1 (two short edges are folded, two are flat). This model will be studied elsewhere.

The most general model with K_1 and K_2 arbitrary forces us to go back to the initial degrees of freedom of the folding model. As we have just seen, the 28 Vertex model allows only for including a bending rigidity for short edges. Introducing a rigidity for long edges as well will introduce an interaction between neighboring vertices, and force us to disentangle the first vertex in Fig.10, and to rather use the $V_2 = 32$ Vertex model formulation of Sect.6.4 (see (6.11)). This new interacting model has a more sophisticated transfer matrix, as the vertices interact with their nearest neighbors.

The two particular limits $K_1 \to \infty$, K_2 finite, or $K_2 \to \infty$, K_1 finite of the general model can be easily solved. They correspond to the complete flattening of one type of edges, thus forming rigid square faces, which can be folded along the other type of edges. This is then equivalent to the folding of the square lattice, whose very simple phase diagram was studied in [9]. The main result was a first order phase transition between a completely flat phase and a completely folded one. What makes the model very simple is the absence of folding entropy, as all the folds initiated on the boundary of the studied domain propagate all the way through the lattice along straight lines. Note that there are $N/2$ flattened squares in the first case (each square is made of 2 triangles), whereas there are $N/4$ such squares in the second case (each square is made of four triangles). The corresponding free energies read

$$\begin{aligned} K_1 \to \infty \ : \ -\frac{f_{K_1,K_2}}{kT} \ &\simeq \ \frac{K_1}{2} + |K_2| \\ K_2 \to \infty \ : \ -\frac{f_{K_1,K_2}}{kT} \ &\simeq \ K_2 + \frac{|K_1|}{2} \end{aligned} \tag{9.9}$$

9.3. Fluid Membrane Folding

We would like to finally comment on a fluid version of the models studied in this paper. A fluid membrane can be modelled by a random tessellation of a Riemann surface. This amounts to replacing the regular lattices representing the tethered membrane by random tessellations with the same type of tiles as the regular lattice, but with an arbitrary connectivity at each vertex.

In the case of the square-diagonal lattice, let us choose for tiles the square faces of S, each made of 4 triangles. In the W_d Vertex formulation of the d-FCH folding, each of these faces is replaced by a 4-valent vertex, with edge values $a \in \mathbb{Z}_{2d}$. This suggests to

introduce a fluid version thereof, in which the lattice is replaced by ϕ^4 (4-valent) graphs, with edge variables $a \in \mathbb{Z}_{2d}$. A simple way of representing the partition function of such a model is to consider a Hermitian multi-matrix integral

$$Z(N,g) \;=\; \int dM_0 ... dM_{2d-1} e^{-N \,\mathrm{Tr}(V(M_0,...,M_{2d-1}))} \tag{9.10}$$

where M_0, M_2, ...,M_{2d-1} are $N \times N$ Hermitian matrices, integrated wrt the standard Haar measure, and

$$\begin{aligned} V(M_0,...,M_{2d-1}) \;&=\; \sum_{i=0}^{2d-1} (\frac{1}{2g} M_i^2 + \frac{d-1}{2} M_i^4) \\ &+ \frac{1}{4} \sum_{0 \le i \ne j \le d-1} (M_i^2 M_j^2 + 2 M_{i+d}^2 M_j^2 + M_{i+d}^2 M_{j+d}^2 + 4 M_i M_j M_{i+d} M_{j+d}) \end{aligned} \tag{9.11}$$

where the quartic terms reproduce the vertices of Fig.18. Moreover, the measure of integration is normalized so that $\lim_{g \to 0} Z(N,g) = 1$. The perturbative expansion of $\mathrm{Log}Z$ as a power series of g and N reads $\mathrm{Log}Z = \sum_{h,n \ge 0} N^{2-2h} g^n Z_{n,h}$, where $Z_{n,h}$ is the partition function for the W_d Vertex model on the set of connected tessellations of surfaces of genus h with n squares. Unfortunately, even for $d = 2$ the solution of the model (9.10) is not known.

Acknowledgements

We thank K. Hallowell for interesting discussions. This work was partially supported by NSF grant PHY-9722060.

References

[1] Y. Kantor and D.R. Nelson, *Crumpling Transition in Polymerized Membranes*, Phys. Rev. Lett. **58** (1987) 2774 and *Phase Transitions in Flexible Polymeric Surfaces*, Phys. Rev. **A 36** (1987) 4020.

[2] D.R. Nelson and L. Peliti, *Fluctuations in Membranes with Crystalline and Hexatic Order*, J. Physique **48** (1987) 1085.

[3] M. Paczuski, M. Kardar and D.R. Nelson, *Landau Theory of the Crumpling Transition*, Phys. Rev. Lett. **60** (1988) 2638.

[4] F. David and E. Guitter, *Crumpling Transition in Elastic Membranes: Renormalization Group Treatment*, Europhys. Lett. **5** (1988) 709.

[5] M. Baig, D. Espriu and J. Wheater, *Phase Transitions in Random Surfaces*, Nucl. Phys. **B314** (1989) 587; R. Renken and J. Kogut, *Scaling Behavior at the Crumpling Transition*, Nucl. Phys. **B342** (1990) 753; R. Harnish and J. Wheater, *The Crumpling Transition of Crystalline Random Surfaces*, Nucl. Phys. **B350** (1991) 861; J. Wheater and P. Stephenson, *On the Crumpling Transition in Crystalline Random Surfaces*, Phys. Lett. **B302** (1993) 447.

[6] P. Di Francesco, O. Golinelli and E. Guitter, *Meander, Folding and Arch Configurations*, Mathl. Comput. Modelling, Vol. **26**, No.8-10 (1997) 97-147, *Meanders and the Temperley-Lieb Algebra*, Commun. Math. Phys. **186** (1997), 1-59 and *Meanders: a direct enumeration approach*, Nucl. Phys. **B482[FS]** (1996), 497-535; P. Di Francesco, *Meander Determinants*, to appear in Commun. Math. Phys. (1998)

[7] Y. Kantor and M.V. Jarić, Europhys. Lett. **11** (1990) 157.

[8] P. Di Francesco and E. Guitter *Entropy of Folding of the Triangular Lattice*, Europhys. Lett. **26** (1994) 455.

[9] P. Di Francesco and E. Guitter *Folding Transition of the Triangular Lattice*, Phys. Rev. **E50** (1994) 4418-4426.

[10] M. Bowick, P. Di Francesco, O. Golinelli and E. Guitter *3D Folding of the triangular lattice*, Nucl. Phys. **B450[FS]** (1995) 463-494.

[11] H. Temperley and E. Lieb, *Relations between the Percolation and Coloring Problems and other Graph-Theoretical Problems associated with regular Planar Lattices: Some Exact Results for the Percolation Problem*, Proc. Roy. Soc. **A322** (1971) 251-280; see also the book by P. Martin, *Potts Models and Related Problems in Statistical Mechanics*, World Scientific, Singapore (1991) for a review.

[12] R.J. Baxter, *Exactly Solved Models in Statistical Mechanics*, Academic Press, London (1982).

[13] P. Di Francesco, B. Eynard and E. Guitter, *Coloring Random Triangulations*, cond-mat/9711050, to appear in Nucl. Phys. **B** (1998).